Tectonics

RESEARCH ARTICLE
10.1029/2020TC006144

Special Section:
Tethyan Dynamics: from Rifting to Collision

Mesozoic Subduction Accretion History in Central Tibet Constrained From Provenance Analysis of the Mugagangri Subduction Complex in the Bangong-Nujiang Suture Zone

Anlin Ma[1,2], Xiumian Hu[1], Paul Kapp[3], Wen Lai[1], Zhong Han[1,2], and Weiwei Xue[1]

[1]State Key Laboratory of Mineral Deposit Research, School of Earth Sciences and Engineering, Nanjing University, Nanjing, China, [2]State Key Laboratory of Oil and Gas Reservoir Geology and Exploitation, Chengdu University of Technology, Chengdu, China, [3]Department of Geosciences, University of Arizona, Tucson, AZ, USA

Abstract The Mugagangri Complex in central Tibet provides a record of the subduction accretion history between the Lhasa and Qiangtang terranes and consists of coherent sedimentary sequences, strongly dismembered formations, and siliciclastic-matrix block-in-matrix mélange. We identified three different groups of sandstone within the Mugagangri Complex. Group 1 is volcaniclastic lithic ($Q_{41}F_{19}L_{40}$, $Lm_{16}Lv_{77}Ls_{7}$) and exhibits youngest U-Pb detrital zircon (YDZ) ages of 177–170 Ma. Group 2 is litho-quartzose ($Q_{67}F_{6}L_{27}$, $Lm_{23}Lv_{63}Ls_{13}$) with YDZ ages of 237–213 Ma. Groups 1 and 2 show provenance affinity with the Qiangtang terrane to the north. Group 3 is similar to Group 2 in detrital mode ($Q_{67}F_{2}L_{31}$) and U-Pb detrital zircon age spectra but is distinguished by more sedimentary fragments ($Lm_{17}Lv_{24}Ls_{59}$), a 1,200–1,100 Ma age peak that is possibly characteristic of the Lhasa terrane to the south and YDZ ages of 284–246 Ma. During (and possibly prior to) Late Triassic time, the recycled orogen-derived sandstones, including Group 2 and possibly Group 3, were deposited on the ocean floor adjacent to the Qiangtang terrane. During the early Middle Jurassic, the arc-derived sandstone (Group 1) was deposited and accreted through the northward subduction of Bangong-Nujiang oceanic lithosphere. During the late Middle to Late Jurassic, Groups 2 and 3 may have been deposited in a trench or trench slope basin, with Group 3 receiving detritus from both the Lhasa and Qiangtang terranes. These three groups of sandstone and ocean plate stratigraphy were mixed in the mélange during the accretion between the Lhasa and Qiangtang terranes.

Key Points:
- The Mugagangri Complex includes subduction complex rocks with three groups of sandstone of distinct provenance
- The sandstones are interpreted to have been deposited and accreted during three periods in the Mesozoic
- The sandstones and ocean plate stratigraphy were structurally mixed in the mélange prior to and perhaps during Lhasa-Qiangtang collision

Supporting Information:
- Supporting Information S1

Correspondence to:
X. Hu,
huxm@nju.edu.cn

Citation:
Ma, A., Hu, X., Kapp, P., Lai, W., Han, Z., & Xue, W. (2020). Mesozoic subduction accretion history in central Tibet constrained from provenance analysis of the Mugagangri Subduction Complex in the Bangong-Nujiang suture zone. *Tectonics*, *39*, e2020TC006144. https://doi.org/10.1029/2020TC006144

Received 28 FEB 2020
Accepted 24 AUG 2020
Accepted article online 26 AUG 2020

©2020. American Geophysical Union. All Rights Reserved.

1. Introduction

The Himalayan-Tibetan orogen formed by the southward younging accretion of continental terranes and subduction complex rocks throughout Phanerozoic time (Dewey et al., 1988; Yin & Harrison, 2000). Many studies have investigated the history of terrane assembly within the Himalayan-Tibetan orogen (e.g., DeCelles et al., 2014; Hu et al., 2016; Kapp et al., 2007; Kapp & DeCelles, 2019; Murphy et al., 1997; Yin & Harrison, 2000). However, there remains much debate about the history of subduction and accretion of subduction complex rocks within well-established and hypothesized suture zones, including the Triassic blueschist- and eclogite-bearing mélanges in central Qiangtang (e.g., Kapp et al., 2003; Liang et al., 2012), the Mugagangri Complex (previously termed as the Mugagangri Group) in the Bangong-Nujiang suture zone (Fan, Li, Liu, & Xu, 2015; Huang et al., 2017; S. Li, Ding, et al., 2017; Zeng et al., 2016) and the Xiukang subduction complex in the Yarlung suture zone (An et al., 2017; Cai et al., 2012; Metcalf & Kapp, 2017, 2019; Wang et al., 2018) (Figure 1a).

The Mugagangri Complex is exposed along a >1,500-km-long east-west belt and consists of mainly siliciclastic-matrix mélange, strongly dismembered formations, and coherent turbiditic sandstone sequences along the Bangong-Nujiang suture zone in central Tibet (Figure 1a). Previous studies in the Gaize (Fan, Li, Liu, et al., 2015; Huang et al., 2017; S. Li, Ding, et al., 2017; Zeng et al., 2016), Nima (C. Li, Wang, et al., 2019), and Dongqiao (S. M. Li et al., 2020) areas (Figure 1a) concluded that all sandstones in the Mugagangri Complex were sourced from the Qiangtang terrane (Fan, Li, Liu, et al., 2015; Huang et al., 2017; S. Li, Ding, et al., 2017; Zeng et al., 2016). However, the tectonic setting in which clastic sedimentary rocks of the Mugagangri Complex were deposited is debated. Some authors interpreted rocks in the Mugagangri

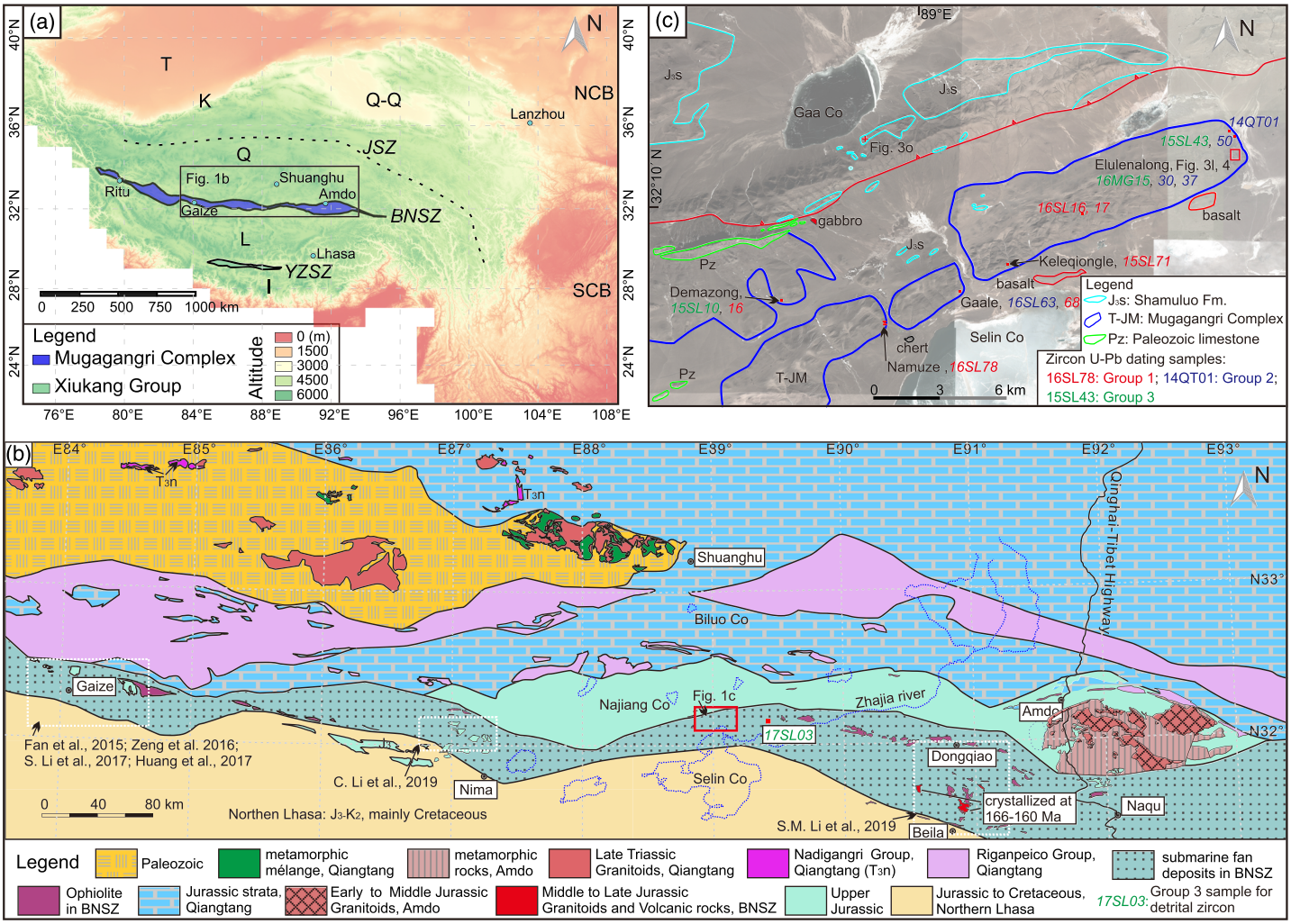

Figure 1. (a) Digital elevation map showing accreted terranes and suture zones in Tibet; (b) simplified geological map after Zhu et al. (2016); (c) geological map of the study area north of Selin Co, with Google Earth satellite image as the base map. T = Tarim; Q-Q = Qilian-Qaidam terrane; K = Kunlun terrane; QT = Qiangtang terrane; L = Lhasa terrane; NCB = North China block; SCB = South China block; I = India block; JSZ = Jinsha suture zone; BNSZ = Bangong-Nujiang suture zone; YZSZ = Yarlung suture zone. Co means lake in Tibetan.

Complex mainly as disrupted forearc basin and accretionary prism rocks related to the northward subduction of the Bangong-Nujiang Tethyan oceanic lithosphere beneath the Qiangtang terrane during the Late Triassic to Jurassic, or even as late as the Early Cretaceous (Fan, Li, Liu, et al., 2015; Huang et al., 2017; S. Li, Ding, et al., 2017; C. Li, Wang, et al., 2019; S. M. Li et al., 2020; Zeng et al., 2016). Additionally, some authors interpreted the Mugagangri Complex to include abyssal plain strata that were deposited along the passive continental margin of the Qiangtang Terrane during the Late Triassic (S. Li, Ding, et al., 2017; Zeng et al., 2016). Differences in interpreted settings and source areas are due to a poor knowledge of the depositional age, the contact relationships between different rock types, and potential along-strike variations in the Mugagangri Complex.

In this study, we present stratigraphic, structural, sedimentological, petrological, and geochronological data from the Mugagangri Complex exposed on the north bank of Selin Co (Co means Lake) (Figures 1b and 1c). We interpret the provenance and depositional ages of the sandstones in the Mugagangri Complex by comparing them with those of potential source rocks in the Qiangtang terrane to the north and in the Lhasa terrane to the south, and also with those along-strike in the Bangong-Nujiang suture zone. We conclude by outlining a possible Mesozoic accretionary history in central Tibet.

2. Geological Background

2.1. Qiangtang Terrane

The Qiangtang terrane is bounded to the north by the Jinsha suture zone and to the south by the Bangong-Nujiang suture zone (Figure 1a). It is further subdivided into northern and southern basins by a NW-SE trending structural culmination composed of Triassic high-pressure metamorphic rocks and Paleozoic ophiolitic mélange (e.g., Kapp et al., 2003; Pullen et al., 2011; Zhai et al., 2016; Zhang et al., 2006). Mesozoic shallow marine and subaerial strata are widespread in the northern and southern Qiangtang basins (XZBGM, 1997). In the southern Qiangtang basin, the Upper Triassic Riganpeico Group consists of sandstone, mudrock, and limestone with a central Qiangtang provenance (Gehrels et al., 2011; Institute of Tibetan Geological Survey, 2006; Ma et al., 2017). The Lower to Middle Jurassic Quse, Sewa, and Buqu formations consist of limestone and shale, volcaniclastic sandstone, and limestone that are interpreted to have been deposited in a forearc basin (Ma et al., 2017; Raterman et al., 2014). The Middle Jurassic Biluoco Formation unconformably overlies the Buqu Formation, consists of recycled-orogen derived detritus, and has been interpreted to be related to Lhasa-Qiangtang collision, flat-slab oceanic subduction, or microcontinent-Qiangtang collision (Ma et al., 2017). The Middle Jurassic Suowa Formation consists of limestone (Ma et al., 2017). All of the Triassic-Jurassic strata were deposited in littoral to shallow marine environments, deformed, and then unconformably overlain by the Upper Cretaceous continental redbeds of the Abushan Formation (XZBGM, 1997; Ma et al., 2017; Institute of Tibetan Geological Survey, 2006; Wang & Fu, 2018).

2.2. Lhasa Terrane

The Lhasa terrane is bounded to the north by the Bangong-Nujiang suture zone and to the south by the Yarlung suture zone (Figure 1a). The strata on the northern part of the Lhasa terrane are dominated by Triassic to Jurassic deep-marine turbiditic clastic rocks (the Upper Triassic Quehala Group, Lower-Middle Jurassic Xihu Group, and Middle-Upper Jurassic Jienu Group), Jurassic to Cretaceous deep- to shallow-marine Lagongtang Formation, Lower Cretaceous shallow marine sedimentary successions (Duoni, Duba and Langshan formations), and Upper Cretaceous continental redbeds (Jingzhushan Formation) (Institute of Tibetan Geological Survey, 2002; Lai, Hu, Garzanti, Sun, et al., 2019; Lai, Hu, Garzanti, Xu, et al., 2019; Leier et al., 2007; G. Sun et al., 2017; Figure 2).

Detrital zircons from pre-Jurassic strata in the Lhasa terrane feature a prominent age peak at 1,250–1,050 Ma and subordinate peaks at 1,650–1,450 and 1,900–1,700 Ma; among <1 Ga zircons, 560 Ma and 300 Ma are the two most prominent age peaks, with subordinate age peaks at 490, 370, 340, and 230 Ma (Gehrels et al., 2011; Leier, Kapp, et al., 2007; G.W. Li et al., 2014; Zhu et al., 2011). This age pattern is different from the Qiangtang terrane where detrital zircon U-Pb ages cluster between 1,100 and 500 Ma, with minor peaks at 2,500, 1,870, 480–400, and 300–200 Ma (Dong et al., 2011; Gehrels et al., 2011; Pullen et al., 2011; Wang, Wu, et al., 2016).

2.3. Bangong-Nujiang Suture Zone

The Bangong-Nujiang suture zone separates the Qiangtang terrane to the north from the Lhasa terrane to the south. Interpreted ophiolitic rocks within the suture zone yield crystallization ages that range from the Triassic to Early Cretaceous (e.g., Bao et al., 2007; Baxter et al., 2009; Fan et al., 2014; Huang et al., 2013, 2015; J. F. Li et al., 2013; Liu et al., 2016; Qu et al., 2010; Shi, 2007; Sun et al., 2011; Tang, Zhai, Hu, Wang, et al., 2018; Tang, Zhai, Hu, Xiao, et al., 2018; Wang, 2000; Wang, Wang, et al., 2016; Wu et al., 2018; Xia et al., 2008; Xu et al., 2014; Zhang et al., 2007, 2014; Zhong et al., 2017; Zhu et al., 2006). The Mugagangri Complex was first established in the Nima area (Figure 1b) as the Mugagangri Group and described as Middle Jurassic flysch (Wen, 1979). Recent studies show that the Mugagangri Complex consists of coherent sedimentary sequences of Qiangtang affinity and siliciclastic mélange that can be divided into several units, including the Early Cretaceous Zhaguo Formation, several Triassic to Jurassic subunits, the Middle Jurassic Gamulong Formation, Dongqiao-Amdo mélange, Daru mélange, and Beila-Naqu mélange (Fan, Li, Liu, et al., 2015; Huang et al., 2017; S. Li et al., 2017; C. Li, Wang, et al., 2019; S. M. Li et al., 2020; Sun et al., 2019; Zeng et al., 2016). The shallow marine Shamuluo Formation (Figure 2) is structurally juxtaposed against the Mugagangri Complex in the Najiangco area; it is composed of sandstone, shale, and limestone and was constrained to be Oxfordian to Kimmeridgian with recycled orogen-derived

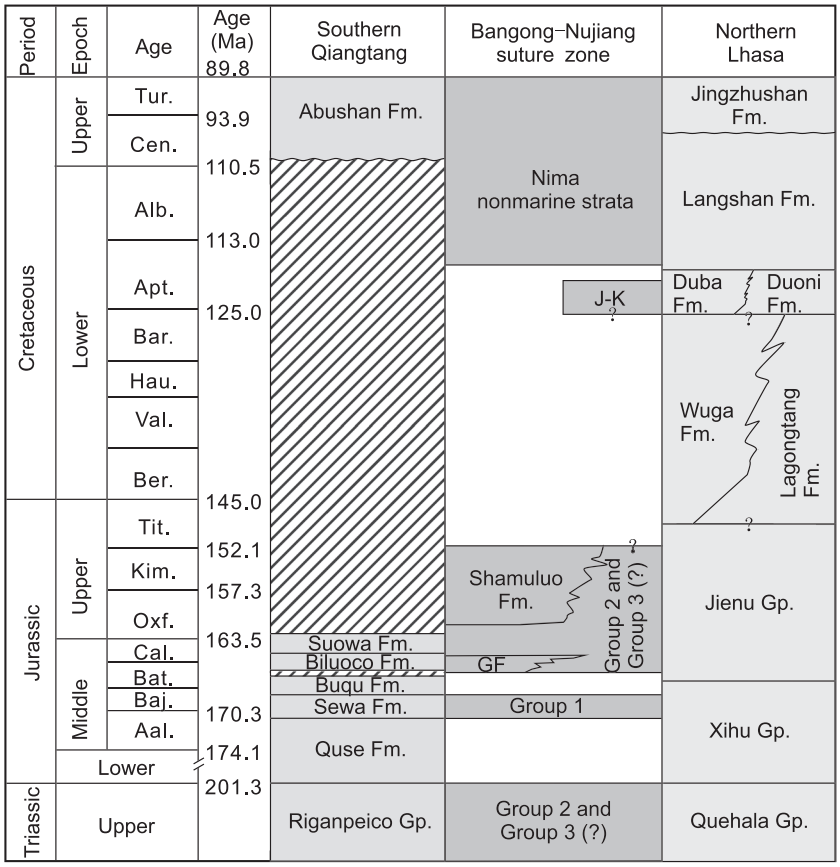

Figure 2. Stratigraphic charts of the southern Qiangtang terrane, the Bangong-Nujiang suture zone, and the northern Lhasa terrane, based on Institute of Tibetan Geological Survey (2002); Kapp et al. (2007); S. Li, Ding, et al. (2017); Ma et al. (2017, 2018); Sun et al. (2019); Lai, Hu, Garzanti, Sun, et al. (2019); and Lai, Hu, Garzanti, Xu, et al. (2019) and age range interpretation of the units in the Mugagangri Complex in this study. GF = Gamulong Formation (Sun et al., 2019). Timescale in Ma is from Cohen et al. (2013).

provenance from the Qiangtang interior (Ma et al., 2018). In the Nima area, deep marine Jurassic (?) to Early Cretaceous (with maximum depositional ages as young as ~125 Ma) turbiditic strata (J-K unit on Figure 2) are unconformably overlain by ~118 Ma and younger nonmarine conglomeratic strata (Kapp et al., 2007).

2.4. Magmatism in Central Tibet

Mesozoic magmatic rocks are scattered throughout the Qiangtang terrane, Bangong-Nujiang suture zone, and central to northern Lhasa terrane (Figures 1b and S1 in the supporting information; data from Chapman & Kapp, 2017). Late Triassic granitoids and volcanic rocks are present within a >400-km-long and ~200-km-wide east-west belt in the central and northern Qiangtang terrane to the west of Shuanghu (Figures 1b and S1). Calc-alkaline intrusions and volcanic rocks with ages of 168–161 and 185–170 Ma are locally exposed in the Gaize to Ritu area along the western part of southern Qiangtang terrane and in Amdo basement, respectively (Figures 1a, 1b, and S1). In addition, 166–160 Ma granitoids and volcanic rocks are present in the Beila area along the Bangong-Nujiang suture zone and 155–135 Ma calc-alkaline igneous rocks are widely distributed in the western part of the central and northern Lhasa terrane (Figure S1). Early Cretaceous magmatic rocks are widespread in the central to northern Lhasa terrane and Bangong-Nujiang suture zone and less abundant but still present in the southern Qiangtang terrane (Figure S1). The region in the southern Qiangtang terrane between Gaize and Amdo was a magmatic-poor continental margin during the Mesozoic (Figures 1b and S1). The tectonic settings of these Mesozoic rocks in central Tibet with respect to closure of the Meso-Tethys (between the Lhasa and Qiangtang terranes) and Neo-Tethys (south of Tibet) are disputed (e.g., Kapp & DeCelles, 2019).

3. Samples and Methods

3.1. Section Measuring and Blocks Counting

The Mugagangri Complex consists dominantly of strongly dismembered formations and mélanges; coherent sedimentary sequences within the Mugagangri Complex are only exposed at a few localities. We measured coherent sedimentary sequences in the Namuze area (see location in Figure 1b) bed by bed in the field to document sedimentary structures and interpret sedimentary environments. Mélanges consisting of blocks in a siliciclastic matrix were documented at four localities in the Seling Co area (Figure 1c). In the Elulenalong area (Figure 1c), we systematically traversed hillsides and documented the lithology of every block in the mélange over 0.1 m in diameter. To avoid repeat counting, we numbered the blocks in order. The GPS locality, lithology, and size of each block were noted (Table S1), and every block is shown as a rectangular body on the map in Figure 4. Eighty samples of sandstone, chert, limestone, and basalt were collected for petrographic analysis (Table S1).

3.2. Sandstone Petrography

At least 300 detrital grains in each sandstone sample ($n = 42$ in total) were point counted under a petrographic microscope following the Gazzi-Dickinson method (Ingersoll et al., 1984; Table S2). The counted and recalculated parameters are modified from Marsaglia and Ingersoll (1992), and the sandstone classification scheme is after Garzanti (2016). Composite thin-section images of each sample under polarized light are provided in the supporting information (Figure S2), which offers an opportunity for automatic point-counting in the future (N. Li, Hao, et al., 2017).

3.3. U-Pb Dating of Detrital Zircons

Fifteen sandstone samples were crushed and processed for heavy minerals by using elutriation and magnetic separation methods. Zircon grains were hand-picked, mounted in epoxy resin, and polished to expose grain centers. U-Pb dating of zircons was conducted using an ICP-MS (Agilent 7500a) coupled to a GeoLas Pro 193-nm laser sampler at the State Key Laboratory of Mineral Deposits Research, Nanjing University, following the methods described by Jackson et al. (2004). A laser beam diameter of 32 μm was used. The laser energy density was 8 J/cm^2 at a frequency of 5 Hz. Zircon standard GEMOC GJ-1, with a $^{207}Pb/^{206}Pb$ age of 608.5 ± 1.5 Ma (Jackson et al., 2004), was used for calibrating the U-Pb fractionation, and zircon standard Mud Tank with an intercept age of 732 ± 5 Ma (Black & Gulson, 1978) was used to monitor accuracy. The GLITTER software (Version 4.4) was used to calculate raw data (www.mq.edu.au/GEMOC). Common Pb correction was conducted following Andersen (2002) to avoid interference from ^{204}Hg in the gas supply. Most of the detrital zircons in the Mugagangri Complex have low U/Th ratios (<10), indicating a magmatic origin (Belousova et al., 2002).

We report $^{206}Pb/^{238}U$ ages for zircon grains <1,000 Ma and $^{207}Pb/^{206}Pb$ ages for grains >1,000 Ma. Zircon analyses >200 Ma with discordance >10%, and those <200 Ma with discordance >20%, were excluded in data presentation and interpretation. The discordance was calculated as ($^{207}Pb/^{235}U$ age − $^{206}Pb/^{238}U$ age)/$^{206}Pb/^{238}U$ age. The software package *Provenance* was used to make Kernel Density Estimation plots of detrital zircon ages (Vermeesch et al., 2016). For age spectrum comparison, we compiled published data. The complete data set from this study is provided in Table S3.

We used multiple methods to calculate the maximum depositional age of the sandstone samples but cite herein the weighted mean age of the youngest two or more grain ages overlapping within 1 σ uncertainty as the maximum depositional age (YC1σ(2+); Tables 1 and S4; Dickinson & Gehrels, 2009).

4. Results

4.1. Stratigraphy and Structural Geology

The mélange in the Selin Co area consists of a matrix of sandstone and mudstone that surrounds both native and exotic blocks. The original texture in siliciclastic rocks in both matrix and blocks, basalt blocks, and blocks of interbedded chert and limestone is well preserved and unmetamorphosed (Figure S3), whereas some limestone and chert blocks are recrystallized. The exotic block is defined as variably sized rock masses occurring in a lithologic association foreign to that in which the mass formed (Berkland et al., 1972). In this study, the chert, limestone, and basalt blocks are tentatively interpreted as fragments of oceanic crust and

Tectonics

10.1029/2020TC006144

Table 1
Youngest Detrital Zircon Ages Calculated for Samples in the Mugagangri Complex

					Youngest detrital zircon age (Ma)							
	Sample	Q:F:L	Lm:Lv:Ls	*n* of DZ	YDZ[a]	YSG[b]	YPP[c]	YC1σ(2+)[d]	YC2σ(3+)[e]	Location	Longitude (°)	Lattitude (°)
Group 1	15SL16	27:46:27	11:83:6	75	171 + 4/−6	172 ± 3	179	174 ± 3 ($n = 4$)	177 ± 3 ($n = 9$)	Demazong	32.129444	88.933056
	15SL71	54:17:29	26:72:2	60	170 + 4/−5	170 ± 2	178	171 ± 25 ($n = 2$)	175 ± 4 ($n = 7$)	Keleqiongle	32.143117	89.043233
	16SL16	38:24:39	4:71:25	30	166 + 6/−7	167 ± 3	169	177 ± 3 ($n = 3$)	177 ± 3 ($n = 3$)		32.164225	89.080092
	16SL17	37:19:44	19:75:4	82	165 + 4/−7	165 ± 3	171	175 ± 4 ($n = 13$)	174 ± 2 ($n = 18$)		32.164225	89.080092
	16SL68	24:16:61	7:87:7	87	168 + 3−/12	169 ± 6	172	170 ± 4 ($n = 12$)	170 ± 4 ($n = 12$)	Gaale	32.132339	89.020653
	16SL78	26:18:56	17:74:8	91	166 + 3/−6	167 ± 3	172	171 ± 1 ($n = 13$)	173 ± 2 ($n = 24$)	Namuze	32.119236	88.983483
Group 2	16MG30	59:3:38	23:28:49	98	210 + 6/−7	211 ± 3	214	213 ± 30 ($n = 2$)	248 ± 8 ($n = 4$)	Elulenalong	32.188283	89.155733
	16MG37	85:3:12	7:79:4	104	202 + 5/−6	203 ± 3	204	213 ± 9 ($n = 7$)	238 ± 15 ($n = 18$)	Elulenalong	32.188336	89.155158
	16SL63	63:12:25	28:60:12	86	208 + 5/−7	209 ± 3	211	214 ± 8 ($n = 4$)	223 ± 11 ($n = 7$)	Gaale	32.133353	89.021400
	15SL50	72:8:20	32:59:10	75	221 + 6/−7	211 ± 3	221	237 ± 9 ($n = 7$)	237 ± 9 ($n = 7$)		32.195317	89.153733
	14QT01	66:3:31	29:66:5	91	202 + 4–7	201 ± 3	210	215 ± 5 ($n = 13$)	230 ± 11 ($n = 24$)	Elulenalong	32.198772	89.152361
Group 3	17SL03	65:3:32	1:39:60	75	213 + 8–8	212 ± 3	212	278 ± 5 ($n = 3$)	278 ± 5 ($n = 3$)		32.150217	89.403367
	15SL43	47:2:51	35:16:48	75	252 + 7/−8	253 ± 4	255	255 ± 6 ($n = 2$)	255 ± 6 ($n = 2$)		32.197033	89.153650
	15SL10	68:4:28	33:10:57	90	276 + 8/−9	276 ± 4	284	284 ± 20 ($n = 3$)	284 ± 20 ($n = 3$)	Demazong	32.128333	88.933611
	16MG15	65:3:32	16:32:53	126	208 + 8/−8	208 ± 4	208	246 ± 5 ($n = 2$)	251 ± 23 ($n = 3$)	Elulenalong	32.187906	89.155694

Note. Samples 15SL16 and 15SL71 are from Ma et al. (2017).
[a]Age calculated by the "Youngest Detrital Zircon" routine of Isoplot (Ludwig, 2008). [b]Youngest single detrital zircon age with 1δ uncertainty. [c]Youngest graphical detrital zircon age peak on an age-probability plot or age-distribution curve. [d]Weighted mean age (±1σ incorporating both internal analytical error and external systematic error) of youngest cluster of two or more grain ages overlapping in age at 1σ. [e]Weighted mean age (±1σ incorporating both internal analytical error and external systematic error) of youngest cluster of three or more grain ages overlapping in age at 2σ (Dickinson & Gehrels, 2009).

Figure 3. (a) Sandstone block in shale-sandstone matrix, Keleqiongle; (b) blocks of thinly interbedded chert and limestone in shale-sandstone matrix, Keleqiongle; (c) close-up of strongly folded chert and limestone block in Figure 3b; (d) scaly fabric in the matrix of sandstone and mudrock, Keleqiongle; (e) blocks of chert and basalt, Demazong; (f) panoramic view of Gaale, showing inferred north dipping thrust fault; (g) native sandstone block in sandstone-shale matrix, Gaale; (h) chert block in dismembered sandstone and shale, Gaale; (i) sandstone blocks in sandstone and mudrock matrix, Gaale; (j) chert and limestone block in matrix of sandstone and mudrock, Gaale; (k) chert block embedded in sandstone matrix, Gaale; (l) block-in-matrix structure in the blocks mapping area, Elulenalong; (m) subhorizontal scaly fabric of the mudrock matrix, with sandstone blocks of various size aligned parallel to the scaly fabric, Elulenalong; (n) sandstone block in scaly mudrock matrix, Elulenalong; (o) limestone from the Shamuluo Formation to the north of the Mugagangri Complex, with felsic intrusions; (p) coherent sequences, Namuze; (q) strongly folded and disrupted coherent sequences, Elulenalong; (r) close-up of relatively coherent sandstone and mudrock layers, Elulenalong.

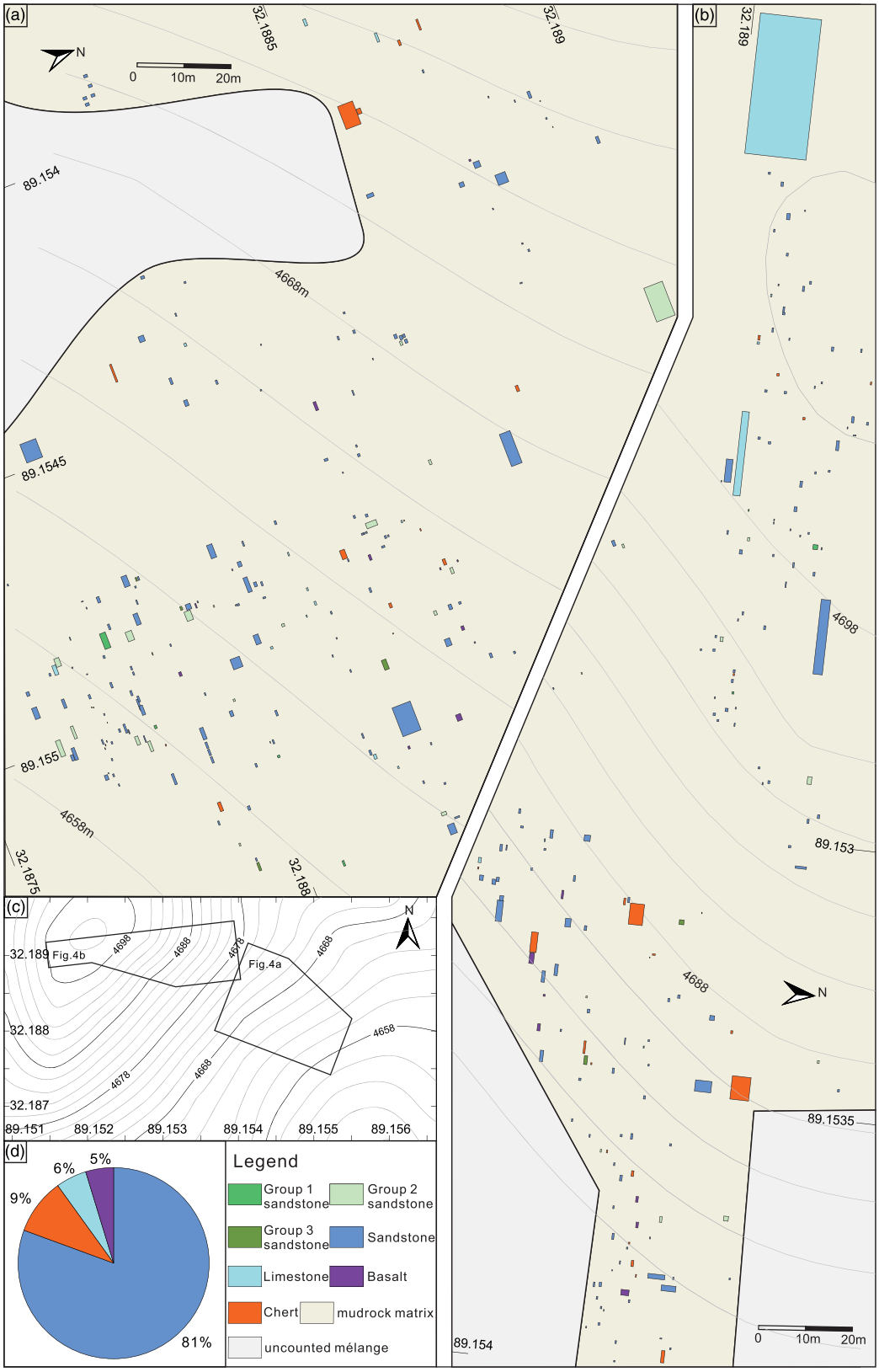

Figure 4. (a, b) Maps of the blocks in mélange, Elulenalong, with legend in (d). Small and large rectangles are abstractive shapes of individual blocks. The foliation/cleavage of mudrock matrix and the long axis of the blocks roughly show an E-W direction; (c) original spatial relationship of (a) and (b); (d) Pie chart showing the percentages of different types of blocks in mélange near Elulenalong.

overlying sedimentary rocks, that is, ocean plate stratigraphy (OPS), and thus are considered to be exotic, as interpreted in many cases (e.g., Raymond, 2019). However, they could be native blocks if the stratigraphic assemblages originally contained chert, limestone, and basalt layers and were subsequently deformed into block-in-matrix mélange (Wakabayashi, 2015).

In the Keleqiongle and Demazong areas (Figure 1c), mélanges with limestone and chert blocks dominate. Volcaniclastic sandstone (Group 1 among three sandstone groups, which are defined based on distinct provenance signatures as detailed below in section 4.3) occurs in the matrix and as blocks (Figure 3a). Group 1 sandstone blocks are mostly <1 m in length, whereas gray-greenish blocks of thinly interbedded and internally folded chert and limestone are locally >10 m in length (Figures 3b and 3c). The matrix of sandstone and mudrock is characterized by a penetrative cleavage (Figure 3d). In the Demazong area (Figure 1c), the mélange includes centimeter- to meter-scale exotic blocks of quartz-rich sandstone (Group 3). Other blocks in the Demazong area mélange include gray-green chert, red chert, and basalt and are structurally dismembered (Figure 3e).

We infer that a north dipping thrust disrupts rock exposures in the Gaale area (Figure 3f). The rocks in Gaale area (Figure 1c) are mainly composed of mélange with blocks of sandstone, chert, and limestone, and sedimentary sequences with broken to strongly dismembered layers (Figures 3g–3k). Volcaniclastic and lithic quartzose sandstone (Groups 1 and 2, respectively) occur both in the matrix and as blocks (Figures 3g–3i). Blocks of thinly interbedded limestone and chert are generally a few meters in length and locally strongly internally folded (Figures 3h, 3j, and 3k).

In the Elulenalong area (Figures 1c and 3l), mélange consists of a matrix of cleaved shale with blocks of sandstone (81%) and minor chert (9%), limestone (6%) and basalt (5%) (Figure 4) oriented parallel to the matrix cleavage (Figures 3m and 3n) according to our systematic mapping of blocks (Figure 4c).

The Mugagangri Complex may include olistostromal (sedimentary) mélange, especially in the Elulenalong are (Figure 3m). However, a tectonic origin cannot be excluded given the strong cleavage in both the blocks and matrix in many areas (e.g., Figures 3a, 3d, 3j, and 3n).

The Mugagangri Complex can be distinguished from strata of the Shamuluo Formation to the north in two aspects. First, the Mugagangri Complex is dominated by mélange and strongly dismembered formations, whereas the strata of the Shamuluo Formation are coherent (Ma et al., 2018). Second, the strata of the Shamuluo Formation are exposed in the hanging wall of a north dipping thrust that juxtaposes more strongly deformed rocks of the Mugagangri Complex in the footwall (Figure 3o); localized limestone massifs on top of the Mugagangri Complex may represent klippen (Figure 1c).

The three groups of sandstone in the Mugagangri Complex show different YDZ ages, which provide constraints on their maximum depositional ages (Table 1). Four sandstone samples from Group 1 in this study along with two published previously (Ma et al., 2017) possess YDZ ages between 177 and 170 Ma. Five sandstone samples from Group 2 show YDZ ages between 237 and 213 Ma. Four sandstone samples from Group 3 yield YDZ ages between 528 and 227 Ma.

4.2. Sedimentology

4.2.1. Description

The Namuze area (Figures 3p and 5) exposes a 108-m-thick coherent sequence of interbedded sandstone, shale, chert, and limestone. The thinly bedded limestone and chert are interbedded with shale in the lower 20 m, with some chert beds folded and enveloped within the limestone beds. The limestone is grainstone with allochems consisting of micrite limestone fragments, minor recrystallized bioclasts, and broken oolites. Thinly bedded and massive sandstones are dominant in the remaining, upper 90 m of the section (Figure 5). The section becomes more structurally disrupted up-section, transitioning into strongly dismembered formation and then siliciclastic-matrix mélange. We interpret the Namuze coherent sequences to have been overthrust southward by siliciclastic-matrix mélange (Figure 3p). In the Elulenalong area, conherent sedimentary sequences with variable degrees of folding and dismemberment consist of thickly to thinly bedded massive sandstone and interbedded shale (Figures 3q and 3r).

In Gaale, Demazong, and Keleqiongle (Figure 1c), sandstone in the matrix is mainly medium, thinly, and medium thinly bedded, respectively, and interbedded with shale; load casts are present at the base of the matrix sandstone layers near Gaale. The limestone blocks near Demazong primarily consist of laminated

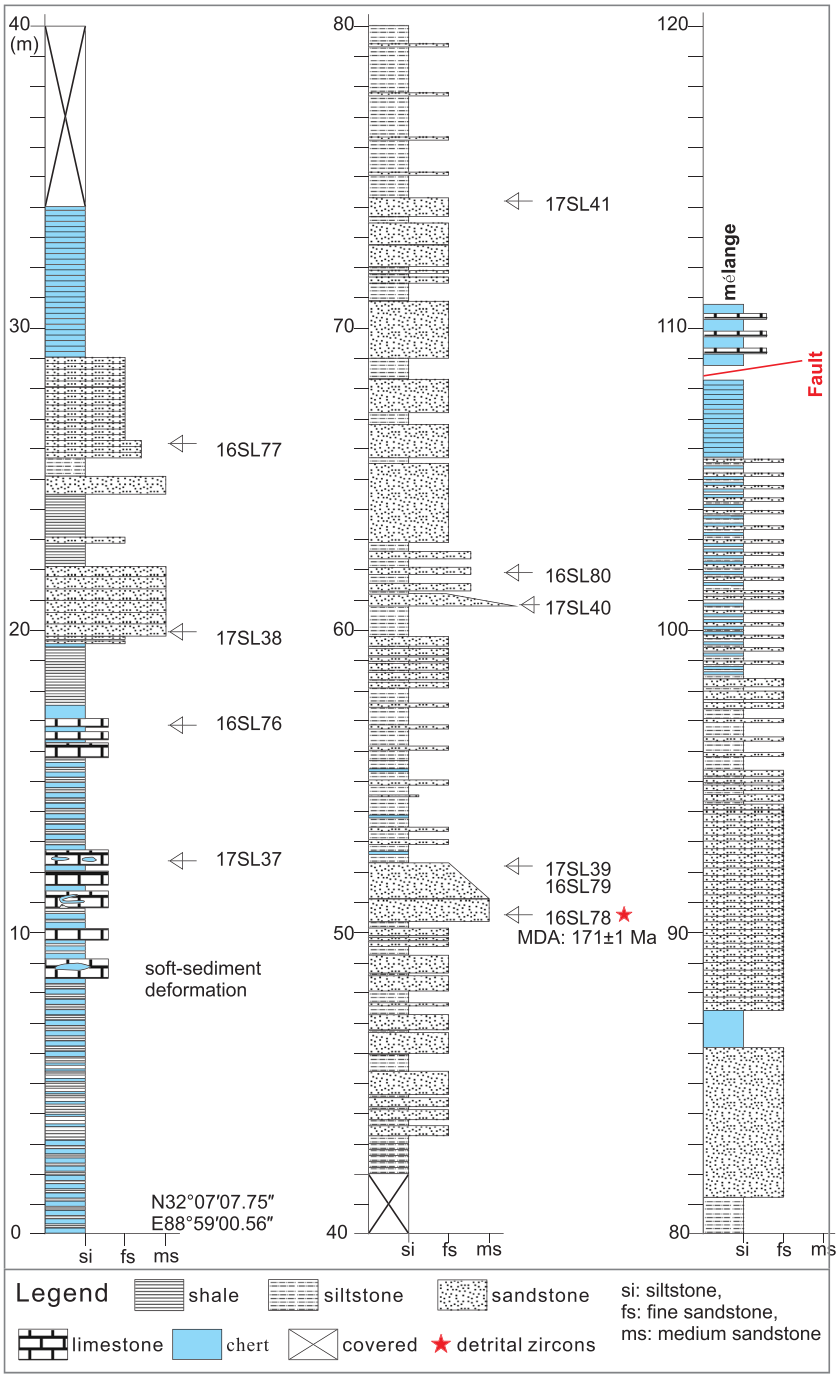

Figure 5. Measured log of the coherent sequences in Namuze area. Arrows denote samples for petrography. MDA = maximum depositional age as constrained by the mean age of two or more of the youngest overlapping detrital zircon ages (see Table 1).

calcisphere packstone, bioclast-bearing micrite limestone, and mixed carbonate and siliciclastic rocks. The limestone blocks near Keleqiongle consist primarily of packstone and wackestone with allochems of micrite limestone fragments, radiolarian, bivalves, and calcisphere grains. Two blocks of chert near Demazong contain radiolarians.

4.2.2. Interpretation

We interpret the sandstones in the Mugagangri Complex to have been deposited in deep marine environments. Massive sandstone with few sedimentary structures implies turbidity flows (Kneller &

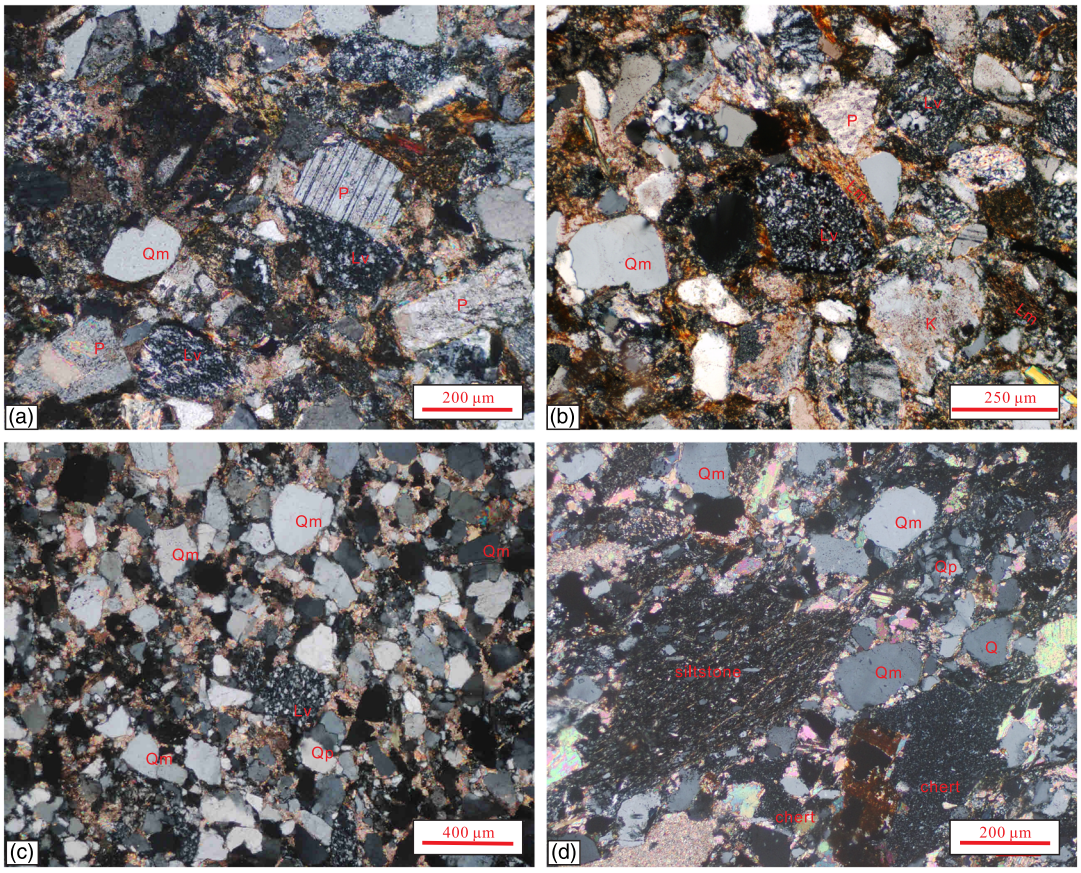

Figure 6. (a, b) Group 1 sandstone with volcaniclastic detritus, Sample 16SL17 as matrix and Sample 17SL40 in coherent sequences in Namuze area, respectively; (c) Group 2 sandstone with abundant quartz, Sample 16MG37 as block in Elulenalong. (d) Group 3 sandstone with sedimentary detritus, Sample 15SL43 as block in Elulenalong area. Qm = monocrystalline quartz; Qp = polycrystalline quartz; P = plagioclase; K = potassium feldspar; Lm = metamorphic fragment; Lv = volcanic fragment.

Branney, 1995). The prevalent and frequently interbedded sandstone and shale are indicative of submarine fan environments, with episodic turbidity flows and changing facies between channel, lobe, levee, and basin plain (Walker, 1978). The micrite limestone and radiolarian chert indicate low-energy marine environments. Well-lithified and rounded limestone grains in the packstone are interpreted as detritus from uplifted marine strata in the source area. Chert inclusions within limestone indicate soft-sediment deformation during diagenesis.

4.3. Provenance Data

Three groups of sandstone with distinct provenance signatures are identified in the Mugagangri Complex. Group 1 is characterized by felsic volcaniclastic sandstone (Figures 6a and 6b). Nine sandstone samples, together with 11 from the literature (Ma et al., 2017), show similar detrital composition with average QFL = 41:19:40 and LmLvLs = 16:77:7 (Figure 7). The quartz grains are mainly monocrystalline, plagioclase is slightly more abundant than K-feldspar (Pl:K ≈ 3:2), and metamorphic lithic fragments are dominated by phyllite. Four sandstone samples in this study and two from Ma et al. (2017) show similar detrital zircon U-Pb age spectra with clusters at 2,500, 1,850, 300–200, and 185–170 Ma (Figure 8). The maximum depositional ages of samples in Group 1 are between 177 and 170 Ma (Table 1).

Group 2 sandstones contain more quartz and less feldspar than Group 1 (Figure 6c), with average QFL = 67:6:27 and LmLvLs = 23:63:13 based on 28 samples (Figure 7). The quartz grains are mainly monocrystalline. The dominant lithic fragments in most samples are felsic volcanic, with subordinate metamorphic fragments including slate, phyllite, and minor schist and sedimentary fragments including shale, siltstone, sandstone, limestone, and chert. Some samples contain more limestone lithics than volcanic lithics

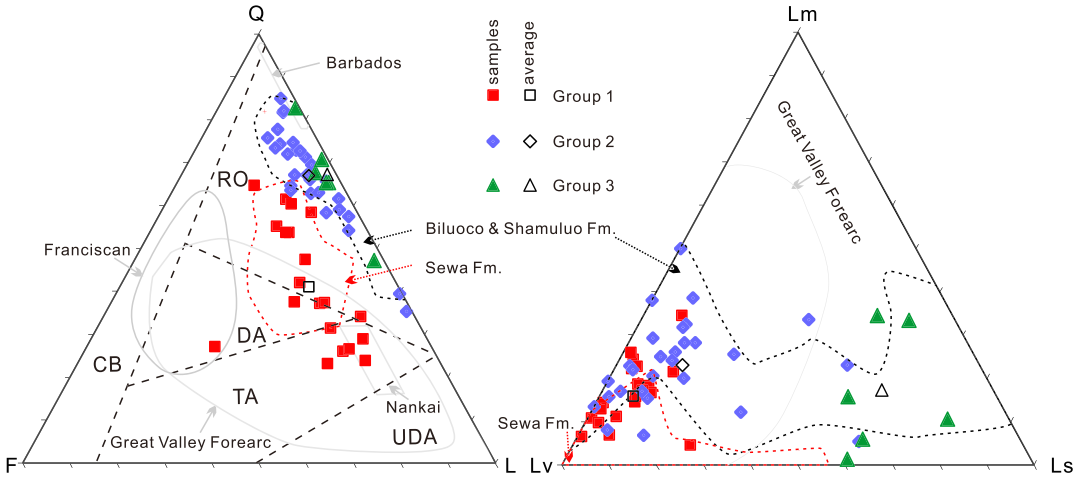

Figure 7. Petrographic ternary diagram of the Mugagangri Complex sandstones and their comparison with the Sewa, Biluoco, and Shamuluo formations to the north (Ma et al., 2017, 2018), as well as the classical accretionary prism sandstones (reviewed by Critelli, 1993, with additional Franciscan QFL data from Dickinson et al., 1982, and Jacobson, 1978, and Great Valley Forearc data from Ingersoll, 1983). Q = quartz; F = feldspar, L = lithic fragments (Lm = metamorphic; Ls = sedimentary; Lv = volcanic); RO = recycled orogen; DA = dissected arc; TA = transitional arc; UDA = undissected arc; CB = continental block.

(e.g., 16MG12). Detrital zircon spectra of five samples from Group 2 show U-Pb age peaks at 2,500, 1,850, 500–960, 470, 450–410, and 200–300 Ma (Figure 8). The maximum depositional ages of samples in Group 2 are between 237 and 217 Ma (Table 1).

Group 3 sandstones are similar to Group 2 sandstones in terms of QFL (average QFL = 67:2:31) but are distinguished by abundant sedimentary fragments (average LmLvLs = 17:24:59) (Figure 7) of chert and terrigenous detritus (Figure 6d). Igneous fragments are mainly felsic, and metamorphic grains are dominated by slate and phyllite. Four samples show similar age spectra, with peaks at 2,500, 1,800–1,600, and 1,200–250 Ma (Figure 8). The maximum depositional ages of samples in Group 3 are between 284 and 246 Ma (Table 1), slightly older than those in Group 2.

5. Discussion

5.1. Sandstone Provenance

Group 1 sandstones were sourced from a magmatic arc. They contain abundant felsic volcaniclastic fragments and feldspar grains (Figure 7) and thus plot in a volcanic arc terrane field in a QFL diagram (Dickinson, 1985). Arc magmatism was likely active during Early-Middle Jurassic time as suggested by the youngest detrital zircon ages between 177 and 170 Ma. These zircons overlap in age with granitoids that intrude into basement rocks in the Amdo area (Figure 1a) and are inferred to have been buried along-strike in the southern Qiangtang terrane (Guynn et al., 2006). Both detrital composition and detrital zircon spectra of the Group 1 sandstones are similar to those of the Sewa Formation in the southern Qiangtang basin (Figures 7 and 9), suggesting they may have been deposited in the same approximately southward palaeodrainage system from shallow marine (Sewa Formation) to deep marine (Group 1) settings. The Group 1 sandstone may be correlated with the Dongqiao-Amdo mélange ~180 km along-strike to the east but is distinct with the Beila-Naqu mélange to the south of the Dongqiao-Amdo mélange, which includes local granitoids and volcanic rocks (S. M. Li et al., 2020; Figures 1 and 9).

Group 2 sandstones have a recycled orogen provenance (Dickinson, 1985; Figure 7). The compositions of lithic fragments suggest that the source includes felsic volcanic, siliciclastic, and low-grade metamorphic rocks. The detrital composition is similar to that of the latest Middle Jurassic Biluoco Formation (deposited at ~166–165 Ma) in the southern Qiangtang basin and Late Jurassic Shamuluo Formation (deposited at ~162–153 Ma) to the north of the Mugagangri Complex (Figure 7). The zircon U-Pb age spectrum is similar to those of the Mugagangri Complex (near Gaize with upper unit [Tma] excluded, near Nima, and near

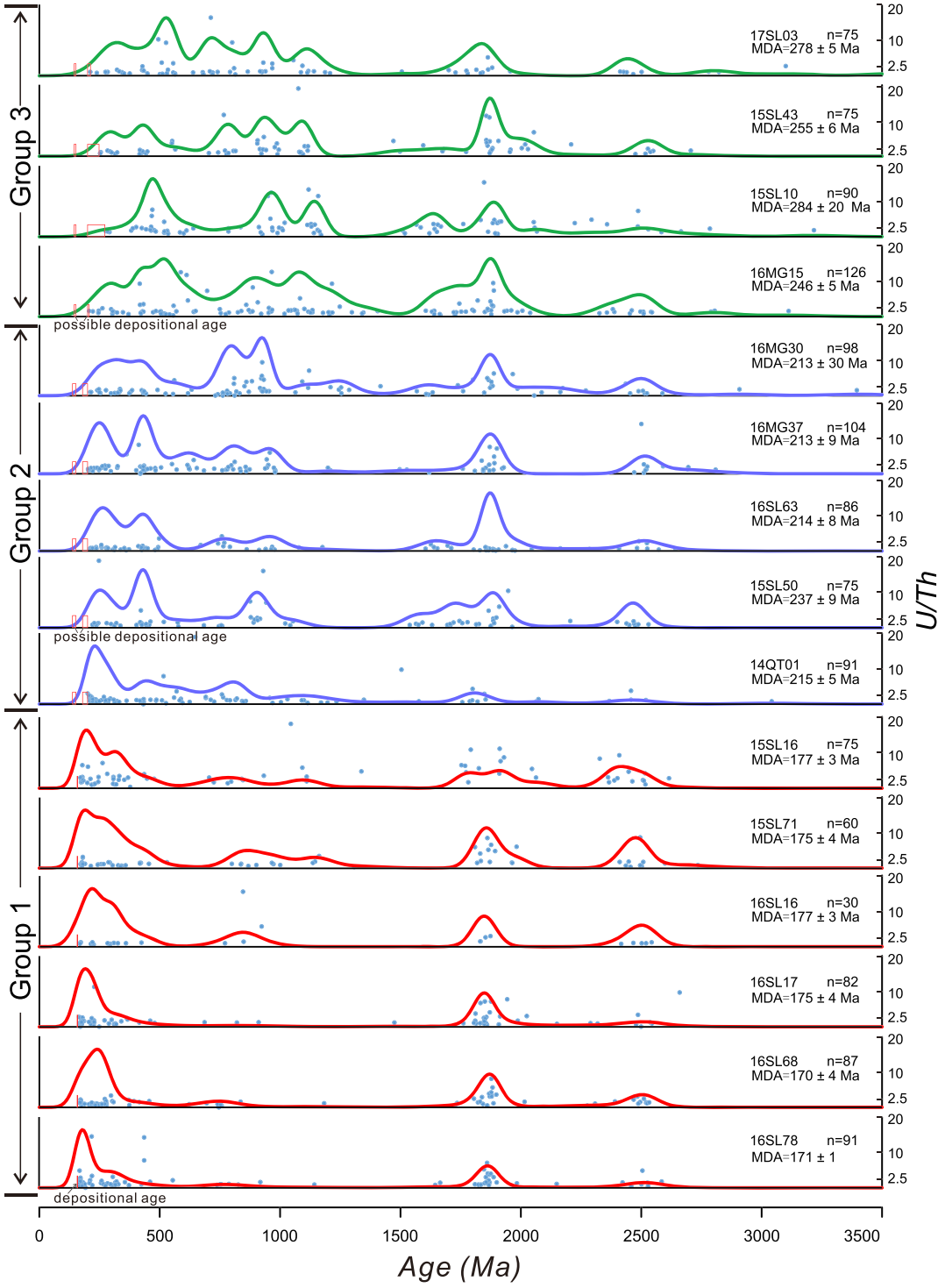

Figure 8. Kernel density estimator plot of the U-Pb ages of the detrital zircons of each sandstone sample from the Mugagangri Complex, with the U/Th ratio of zircons on the right axis. The interpreted depositional age interval of each sample is shown.

Dongqiao as blocks of sandstone in Daru mélange), the Jurassic Biluoco and Shamuluo formations, the Upper Triassic Riganpeico Group in the southern Qiangtang basin, and pre-Jurassic strata in the Qiangtang terrane, but different from pre-Jurassic strata in the Lhasa terrane (Figure 9). The youngest detrital zircon ages between 237 and 213 Ma suggest the rocks in the source area should not contain

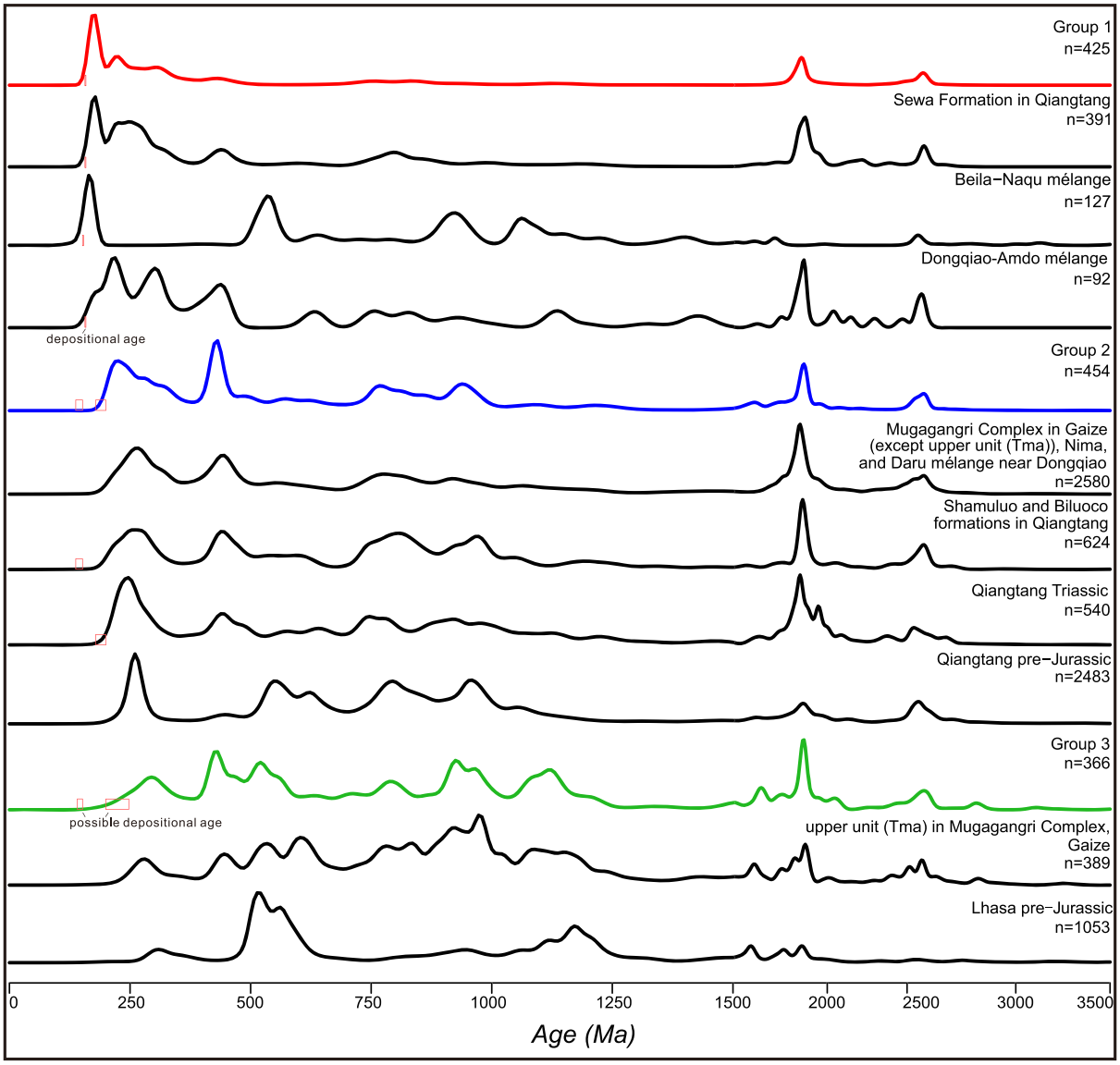

Figure 9. Kernel density estimator plots of detrital zircon U-Pb ages of the Groups 1, 2, and 3 sandstones and their comparison with those of the Sewa Formation, Biluoco and Shamuluo formations in the southern Qiangtang terrane, along-strike Mugagangri complex, Triassic and pre-Jurassic strata of the southern Qiangtang terrane, and pre-Jurassic strata of Lhasa terrane. The Qiangtang data set is from Dong et al. (2011), Gehrels et al. (2011), Ma et al. (2017, 2018), Pullen et al. (2011), and Wang, Wu, et al. (2016); the Lhasa data set is from Gehrels et al. (2011); Leier, Kapp et al. (2007); G.W. Li et al. (2014); and Zhu et al. (2011); the Mugagangri Complex data set is from Huang et al. (2017); C. Li, Wang, et al. (2019); S. Li, Ding, et al. (2017); S.M. Li et al. (2020); and Zeng et al. (2016); the upper unit (Tma) data set in Gaize is from S. Li, Ding, et al. (2017). The (interpreted) depositional age interval of each sample is shown.

zircons younger than the Late Triassic. Consequently, we interpret that Group 2 sandstones were sourced from the central Qiangtang terrane, which experienced extensive volcanism during Late Triassic time and was a topographic high between the northern and southern Qiangtang basins since Late Triassic time (Wang & Fu, 2018).

Group 3 sandstones are compositionally mature (Figure 7) and may have a mixed Lhasa and Qiangtang provenance signal. The high percentage of sedimentary lithic fragments indicates a dominance of sedimentary strata in the source region. The abundant chert clasts could have been sourced from an exhumed ophiolite terrane within the Lhasa or Qiangtang terranes or the Bangong-Nujiang suture zone (e.g., Li, 1987; Yang et al., 2009). The detrital zircon age spectrum of Group 3 is similar to that of Group 2 (Figure 9), implying Qiangtang affinity. Some age peaks including 1,800–1,500, 520, and especially 1,200–1,100 Ma are

indicative of the Lhasa terrane (Figure 9), implying that the Lhasa terrane may also have contributed detritus to the sandstones. However, the Lhasa terrane signature is not that robust, because Group 3 sandstones show a late Mesoproterozoic age peak that is slightly younger than that in the Lhasa terrane (~1.1 Ga vs. ~1.2 Ga) and the late Mesoproterozoic age signature is ubiquitous globally. The detrital zircon age spectrum of Group 3 is similar to that of the upper unit (Tma) in the Mugagangri Complex along-strike to the west in the Gaize area (S. Li, Ding, et al., 2017; Figure 9).

5.2. Deposition and Accretion History

Rare fossils in the Dongqiao, Nima, and Ritu areas (Cao et al., 2008; Wen, 1979; Zeng et al., 2016) and ages of one volcanic interbed in the Gaize area (Fan, Li, Liu, et al., 2015) roughly constrain the depositional age of sedimentary rocks in the Mugagangri Complex to range from Jurassic to Cretaceous. Previously published detrital zircon studies indicate maximum depositional ages of 460–166 Ma according to the YDZ age (Fan, Li, Liu, et al., 2015; Huang et al., 2017; S. Li, Ding, et al., 2017; C. Li, Wang, et al., 2019; S. M. Li et al., 2020; Zeng et al., 2016). In the Selin Co area, the depositional age of the Mugagangri Complex was not well constrained because of the lack of fossils and volcanic layers (Institute of Tibetan Geological Survey, 2006). Here we use YDZ ages to constrain the maximum depositional ages of the Mugagangri Complex and to discuss the history of deposition and accretion of the Mugagangri Complex. Since the Bangong-Nujiang belt extends over 1,500 km from east to west, along-strike geological differences must be considered when reconstructing the deposition and accretion history. In this study, we mainly focus on the Selin Co area, where there is no geological evidence for microcontinent blocks and Jurassic magmatic arc rocks are rarely exposed in the suture zone, southern Qiangtang terrane, and northern part of the Lhasa terrane (Figures 1b and S1).

5.2.1. Late Triassic

The high degree of similarity in both zircon age populations and maximum depositional ages between Group 2 sandstones and the Riganpeico Group (Figure 9; Tables 1 and S4) suggests that there may have existed paleo-drainages connecting the Qiangtang terrane interior with the Bangong-Nujiang Ocean during the Late Triassic (Figures 10a and 10b). Mesozoic sedimentation initiated in the southern Qiangtang terrane during Late Triassic time, with sandstone and limestone of the Riganpeico Group having been deposited in a subaerial to shallow marine basin (Wang & Fu, 2018). The Bangong-Nujiang ocean, which opened prior to the Permian based on paleobiogeography (Zhang et al., 2018), remained open during Middle to Late Triassic time as suggested by the presence of Late Triassic oceanic island arc rocks within the Bangong-Nujiang suture zone (Fan et al., 2017).

Based on the Late Triassic provenance and paleogeography, we propose that Group 2 sandstones were deposited on oceanic crust proximal to the southern continental margin of the Qiangtang terrane (Figure 10a) before it was structurally trapped in proximity to an oceanic subduction zone setting. In Gaize, the sandstones with similar composition to Group 2 were interpreted to have been deposited and accreted in an accretionary prism associated with a subduction zone that was interpreted to have initiated at ~220 Ma (Figure 10b; Zeng et al., 2016) or to have been deposited along a passive continental margin setting prior to subduction initiation at ~195–190 Ma (Figure 10a; S. Li, Ding, et al., 2017; Li, Yin, et al., 2019). In this study, the detrital composition of Group 2 (recycled-orogen-derived) is distinct from typical subduction complex sandstones like those of the Franciscan and Nankai rocks that have an arc provenance (Figure 7) and where subduction initiation was thought to have been intraoceanic (e.g., Stern & Bloomer, 1992; Wakabayashi, 1990; Wakabayashi et al., 2010). We propose subduction of the Bangong-Nujiang ocean may have initiated northward beneath the Qiangtang terrane along a rifted (passive) margin instead of in an intraoceanic setting, which may better explain the interpreted southward paleo-drainage system from the shallow marine southern Qiangtang terrane to the deep marine Bangong-Nujiang ocean to the south, and the final accretion of Group 2 sandstones into subduction complex rocks. Otherwise, the detrital composition of Group 2 is similar with that in the Nias and Barbados subduction complexes in which the trench fill was fed by along-strike sediment transport (Velbel, 1985).

5.2.2. Early to Middle Jurassic

We interpret that Group 1 sandstones were deposited synchronously with the shallow marine Sewa Formation to the north in the southern Qiangtang terrane during early Middle Jurassic time (Figure 10c). This is supported by their similar detrital zircon age spectra and youngest detrital zircon age population (Figure 9; Tables 1 and S4). Group 1 sandstones are interpreted to have been originally deposited in a

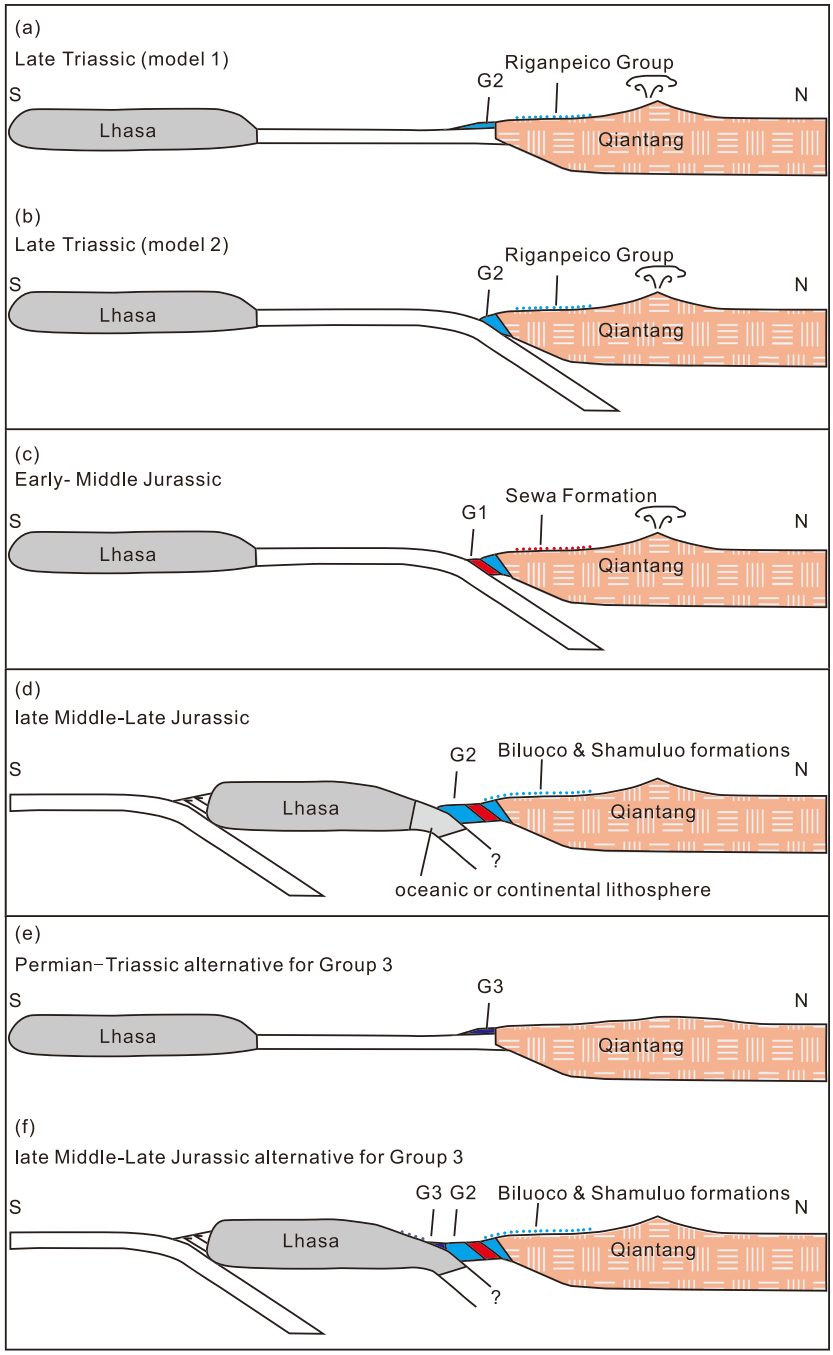

Figure 10. (a and b) Alternative tectonic interpretations during Late Triassic time, with the shallow marine Riganpeico Group deposited in southern Qiangtang: (a) Group 2 sandstone was deposited on the ocean floor attached to the passive southern Qiangtang margin; (b) northward subduction of Bangong-Nujiang ocean initiated and the Group 2 sandstones were deposited in trench or trench slope basins and accreted; (c) during the early Middle Jurassic, Group 1 sandstone was deposited and accreted in a forearc setting, possibly in trench and trench slope basins. At the same time, the Sewa Formation was deposited in the southern Qiangtang basin, and Group 2 was incorporated into the accretionary prism; (d) during late Middle to Late Jurassic time, additional Group 2 sandstone was deposited in a trench area between the Lhasa and Qiangtang terranes, with the Biluoco and Shamuluo formations of the same provenance deposited to the north. At this time, the Lhasa and Qiangtang terranes may or may not have collided; (e) alternative model for Group 3 in which Group 3 was deposited during the Permian-Triassic on oceanic floor adjacent to the southern Qiangtang terrane passive continental margin; (f) alternative model for Group 3 sandstone in which Group 3 was deposited in the trench with mixed provenance from Qiangtang and Lhasa during late Middle to Late Jurassic time. Dash line below stratigraphic units indicates what was being deposited.

trench, or trench slope with respect to the northward subducting Bangong-Nujiang oceanic lithosphere. Within the suture zone, coherent sequences consisting of Group 1 sandstone and interbedded chert, limestone, and shale (in Namuze area) were likely deposited in trench or trench-slope basins. Chert, basalt, and limestone blocks, interpreted as Bangong-Nujiang OPS, are mixed with Group 1 sandstones, suggesting the formation of a subduction complex prism. In a broader perspective, Group 1 sandstones are similar in detrital composition to sandstones in classical subduction prisms such as those in the Nankai Trough and Franciscan subduction complex (Figure 7).

During Early to Middle Jurassic time, the Late Triassic Group 2 sandstones may have been incorporated into the north dipping Bangong-Nujiang oceanic subduction complex (S. Li, Wang, et al., 2019; Zeng et al., 2016). In a progressive accretion model (e.g., Ernst et al., 2009; Seely et al., 1974), the Group 1 sandstone should be accreted beneath the Group 2 sandstone.

5.2.3. Late Middle to Late Jurassic

We interpret that some Group 2 sandstones may have been deposited during late Middle to Late Jurassic time (Figure 10d) as they share similar detrital modes (Figure 7), detrital zircon age spectra (Figure 9), and maximum depositional ages with the late Middle to Late Jurassic Biluoco and Shamuluo formations (Tables 1 and S4) to the north (Ma et al., 2017, 2018). However, the Lhasa and Qiangtang terranes may or may not have collided during late Middle Jurassic time (Ma et al., 2017), leading to contrasting tectonic interpretations for Group 2 deposition and accretion (Figure 10d). If the Lhasa and Qiangtang terranes initially collided during late Middle Jurassic time, Group 2 sandstones would have been deposited in a trough between the Lhasa and Qiangtang terranes in a syn-collisional setting, which could have been comparable to the present-day Timor trough between the northward subducting Australian continental margin and southesatern Asia (Hall, 2011; Tate et al., 2015). If Lhasa-Qiangtang collision occurred later, Group 2 sandstones may have been deposited in a forearc setting with abnormal provenance, perhaps as a result of flat subduction-related orogenesis and associated termination in arc magmatism.

5.2.4. Group 3: Deposition and Accretion Models

Two models are proposed here to interpret the deposition and accretion of Group 3 sandstones. A future determination of the depositional age will tell which one is correct. In the first model, Group 3 sandstone was deposited on oceanic crust attached to the Qiangtang passive margin between Permian and Triassic time as confined by the maximum depositional ages (Table 1), with a Qiangtang terrane provenance (Figure 10e). In this model, the Lhasa-like signature may be a Qiangtang signature that has yet to be identified (S. Li, Ding, et al., 2017). Alternatively, Group 3 may have been deposited during late Middle to Late Jurassic time when the southern Qiangtang and Bangong-Nujiang basin were being filled up with recycled-orogen-derived materials (Biluoco and Shamuluo formations and Group 2 sandstones; Figure 10f) yielding youngest zircon ages between 528 and 227 Ma (Table S4; Ma et al., 2017). The possible presence of both Qiangtang and Lhasa provenance signals in Group 3 sandstone would be consistent with Lhasa-Qiangtang collision. The lack of Late Jurassic and Early Cretaceous zircons in Group 3 and also Group 2 sandstones casts doubt on this interpretation but could potentially be explained by a scarcity or lack of magmatic rocks of this age in the study region (Figures 1b and S1).

5.3. Mixture of Different Units in the Mugagangri Complex

Four lines of evidence suggest the Mugagangri Complex represents subduction complex rocks related to the northward subduction of the Bangong-Nujiang ocean. First, the plate tectonic position of the Mugagangri Complex is within a suture zone. Second, the Mugagangri Complex is more strongly deformed compared to the faulted-bounded coherent strata of the Shamuluo Formation to the north. Third, the inclusion and mixture of possible OPS blocks (chert, basalt, and limestone) and deep marine terrigenous sandstone in blocks and matrix support the interpretation of a subduction complex (e.g., Searle et al., 1987). Fourth, the siliciclastic-matrix mélange of the Mugagangri Complex contains sandstone blocks and matrix equivalent to the coherent deep marine sequences in the Elulenalong (Group 2) and Namuze (Group 1), which are interpreted to have been deposited in trench or trench slope basin settings. An alternative interpretation is that the Mugagangri Complex may represent an olistostromal (sedimentary) mélange that was deposited in a forearc basin and subsequently structurally disrupted (e.g., Wakabayashi, 2017). Geological evidence in support of this possibility, other than the unmetamorphosed nature of the Mugagangri Complex, is presently limited, and we thus tentatively favor a more traditional subduction complex interpretation.

Accretionary prisms with a progressive long-term growth generally follow an oceanward and structurally downward younging polarity as younger sediments are frontally accreted and underthrust older subduction complex rocks in the upper-plate direction (Seely et al., 1974; Simpson, 2010). This has been confirmed in many accretionary complexes, such as the Franciscan (Dumitru et al., 2015), Chugach (Amato et al., 2013), and Japanese Islands (Isozaki et al., 2010). However, in the Mugagangri Complex, the three groups of sandstone and the possible OPS blocks are well mixed. Near Gaale, Groups 1 and 2 sandstones and OPS blocks are mixed along a 400-m-long NE-SW cliff exposure; near Demazong, Group 3 sandstone blocks are mixed together with Group 1 sandstone and OPS blocks; near Elulenalong, the block counting results show that the three groups of sandstone as well as OPS blocks are well mixed (Figures 4a and 4b).

We interpret the mixture of different types of blocks in the Mugagangri Complex mélange to have occurred mainly in two stages. The first stage took place during the northward oceanic lithosphere subduction during possibly Late Triassic to early Middle Jurassic time (or even later depending on the collision timing of Lhasa and Qiangtang terranes), which leads to Groups 1 and 2 sandstones of Qiangtang affinity to amalgamate with possible OPS and possibly Group 3 sandstone of both Qiangtang and Lhasa affinities. The second stage happened during the Lhasa-Qiangtang collisional processes, loosely constrained to have initiated between the late Middle Jurassic and Early Cretaceous (Fan, Li, Xie, et al., 2015; Girardeau et al., 1984; Kapp et al., 2007; S. Li, Yin, et al., 2019; Ma et al., 2017, 2020; Sun et al., 2019; Zhu et al., 2016). This caused the newly deposited Group 2 sandstones and possibly Group 3 sandstones to mix with former subduction complex rocks by various disruption mechanisms including cataclasis associated with decollement development and out-of-sequence fault zones, mud diapirism, and mass wasting processes that are common in collisional mélanges (Harris et al., 1998).

6. Conclusions

1. The Mugagangri Complex in the Selin Co area contains coherent sedimentary sequences, dismembered formations, and mélange. The mélange is composed of a sandstone and shale matrix that includes blocks of sandstone and subordinate chert, limestone, and basalt. The coherent sedimentary sequences were deposited in deep water basins.
2. Three groups of sandstone are found in the Mugagangri Complex based on sandstone petrography and detrital zircon U-Pb ages. Group 1 sandstone is volcaniclastic and continental arc-derived with maximum depositional ages of 177–170 Ma; Group 2 sandstone is recycled orogen-derived with maximum depositional ages of 237–213 Ma. Both groups are of Qiangtang affinity and present in both coherent sequences and mélange. Group 3 sandstones are compositionally mature and of recycled orogen-derived Qiangtang terrane provenance but with possibly an additional Lhasa terrane provenance; its maximum depositional ages are 284–246 Ma.
3. We propose three deposition and accretion stages in central Tibet during Late Triassic to Late Jurassic time. During the Late Triassic, some Group 2 sandstone was deposited on the ocean floor attached to the continental margin of the Qiangtang terrane. During the early Middle Jurassic, Group 1 sandstone was deposited and accreted in a forearc setting due to the northward subduction of the Bangong-Nujiang oceanic lithosphere. During late Middle Jurassic to Late Jurassic time, additional Group 2 sandstone was deposited along the continental margin of the Qiangtang terrane. Group 3 sandstone may be interpreted as Permian-Triassic passive margin strata deposited on the ocean floor adjacent to the continental margin of the Qiangtang terrane or as upper Mesozoic remnant deep marine strata that were deposited during the Lhasa-Qiangtang collision.
4. The three groups of sandstone and blocks of chert, limestone, and basalt are well mixed in the Mugagangri Complex as a result of long-term convergence prior to and perhaps during the continental collision between the Lhasa and Qiangtang terranes.

Data Availability Statement

The data supporting this paper are available in the supporting information file and Open Science Framework (https://osf.io/zpqdt/).

Acknowledgments

We thank Bin Wu for help with the laser ablation analyses and Yani Najman for assistance and discussion in the field. We thank Kathryn Metcalf for discussion and help with editing the manuscript. We are grateful to Taylor Schildgen and Marco G. Malusa for efficient handling and John Wakabayashi and Peter Cawood for their critical reviews. This work was financially supported by the National Natural Science Foundation of China (Grants 91755209 and 41761130076), the UK Royal Society (Grant NA160334), and the Open Research Funds from the State Key Laboratory for Mineral Deposits Research, Nanjing University (2020-LAMD-K07).

References

Amato, J. M., Pavlis, T. L., Clift, P. D., Kochelek, E. J., Hecker, J. P., Worthman, C. M., & Day, E. M. (2013). Architecture of the Chugach accretionary complex as revealed by detrital zircon ages and lithologic variations: Evidence for Mesozoic subduction erosion in south-central Alaska. *Bulletin*, *125*(11–12), 1891–1911. https://doi.org/10.1130/B30818.1

An, W., Hu, X., & Garzanti, E. (2017). Sandstone provenance and tectonic evolution of the Xiukang Mélange from Neotethyan subduction to India–Asia collision (Yarlung-Zangbo suture, south Tibet). *Gondwana Research*, *41*, 222–234. https://doi.org/10.1016/j.gr.2015.08.010

Andersen, T. (2002). Correction of common lead in U-Pb analyses that do not report 204Pb. *Chemical Geology*, *192*(1–2), 59–79. https://doi.org/10.1016/S0009-2541(02)00195-X

Bao, P., Xiao, X., Su, L., & Wang, J. (2007). Petrological, geochemical and chronological constraints for the tectonic setting of the Dongco ophiolite in Tibet. *Science in China Series D: Earth Sciences*, *50*(5), 660–671. https://doi.org/10.1007/s11430-007-0045-5

Baxter, A. T., Aitchison, J. C., & Zyabrev, S. V. (2009). Radiolarian age constraints on Mesotethyan ocean evolution, and their implications for development of the Bangong-Nujiang suture, Tibet. *Journal of the Geological Society*, *166*(4), 689–694. https://doi.org/10.1144/0016-76492008-128

Belousova, E., Griffin, W. L., O'Reilly, S. Y., & Fisher, N. (2002). Igneous zircon: Trace element composition as an indicator of source rock type. *Contributions to Mineralogy and Petrology*, *143*(5), 602–622. https://doi.org/10.1007/s00410-002-0364-7

Berkland, J. O., Raymond, L. A., Kramer, J. C., Moores, E. M., & O'day, M. (1972). What Is Franciscan? *AAPG Bulletin*, *56*(12), 2295a–2302a.

Black, L., & Gulson, B. (1978). The age of the mud tank carbonatite, strangways range, northern territory. *Journal of Australian Geology and Geophysics*, *3*, 227–232.

Cai, F., Ding, L., Leary, R. J., Wang, H., Xu, Q., Zhang, L., & Yue, Y. (2012). Tectonostratigraphy and provenance of an accretionary complex within the Yarlung–Zangpo suture zone, southern Tibet: Insights into subduction–accretion processes in the Neo-Tethys. *Tectonophysics*, *574-575*, 181–192. https://doi.org/10.1016/j.tecto.2012.08.016

Cao, S., Xiao, X., & Ouyang, K. (2008). Re-new-establishment of the Jurassic Mugagangri Groups and its geological significance on the western side of the Bangong Co-Nujiang Junction Zone (in Chinese with English abstract). *Acta Sedimentologica Sinica*, *26*(4), 559–564.

Chapman, J. B., & Kapp, P. (2017). Tibetan magmatism database. *Geochemistry, Geophysics, Geosystems*, *18*, 4229–4234. https://doi.org/10.1002/2017GC007217

Cohen, K. M., Finney, S. C., Gibbard, P. L., & Fan, J.-X. J. E. (2013). The ICS international chronostratigraphic chart. *Episodes*, *36*(3), 199–204.

Critelli, S. (1993). Sandstone detrital modes in the Paleogene Liguride Complex, accretionary wedge of the southern Apennines (Italy). *Journal of Sedimentary Research*, *63*(3), 464–476. https://doi.org/10.1306/D4267B27-2B26-11D7-8648000102C1865D

DeCelles, P. G., Kapp, P., Gehrels, G. E., & Ding, L. (2014). Paleocene-Eocene foreland basin evolution in the Himalaya of southern Tibet and Nepal: Implications for the age of initial India-Asia collision. *Tectonics*, *33*, 824–849. https://doi.org/10.1002/2014TC003522

Dewey, J. F., Shackleton, R. M., Chengfa, C., & Yiyin, S. (1988). The tectonic evolution of the Tibetan Plateau. *Philosophical Transactions of the Royal Society of London A: Mathematical, Physical and Engineering Sciences*, *327*(1594), 379–413. https://doi.org/10.1098/rsta.1988.0135

Dickinson, W. R. (1985). Interpreting provenance relations from detrital modes of sandstones. In *Provenance of arenites* (pp. 333–361). Dordrecht: Springer.

Dickinson, W. R., & Gehrels, G. E. (2009). Use of U-Pb ages of detrital zircons to infer maximum depositional ages of strata: A test against a Colorado Plateau Mesozoic database. *Earth and Planetary Science Letters*, *288*(1–2), 115–125. https://doi.org/10.1016/j.epsl.2009.09.013

Dickinson, W. R., Ingersoll, R. V., Cowan, D. S., Helmold, K. P., & Suczek, C. A. (1982). Provenance of Franciscan graywackes in coastal California. *Geological Society of America Bulletin*, *93*(2), 95–107. https://doi.org/10.1130/0016-7606(1982)93<95:POFGIC>2.0.CO;2

Dong, C. Y., Li, C., Wan, Y. S., Wang, W., Wu, Y. W., Xie, H. Q., & Liu, D. Y. (2011). Detrital zircon age model of Ordovician Wenquan quartzite south of Lungmuco-Shuanghu Suture in the Qiangtang area, Tibet: Constraint on tectonic affinity and source regions. *Science China Earth Sciences*, *54*(7), 1034–1042. https://doi.org/10.1007/s11430-010-4166-x

Dumitru, T. A., Ernst, W. G., Hourigan, J. K., & McLaughlin, R. J. (2015). Detrital zircon U-Pb reconnaissance of the Franciscan subduction complex in northwestern California. *International Geology Review*, *57*(5–8), 767–800. https://doi.org/10.1080/00206814.2015.1008060

Ernst, W., Martens, U., & Valencia, V. (2009). U-Pb ages of detrital zircons in Pacheco Pass metagraywackes: Sierran-Klamath source of mid-Cretaceous and Late Cretaceous Franciscan deposition and underplating. *Tectonics*, *28*, TC6011. https://doi.org/10.1029/2008TC002352

Fan, J.-J., Li, C., Liu, Y.-M., & Xu, J.-X. (2015). Age and nature of the late Early Cretaceous Zhaga Formation, northern Tibet: Constraints on when the Bangong–Nujiang Neo-Tethys Ocean closed. *International Geology Review*, *57*(3), 342–353. https://doi.org/10.1080/00206814.2015.1006695

Fan, J.-J., Li, C., Wang, M., Liu, Y.-M., & Xie, C.-M. (2017). Remnants of a Late Triassic ocean island in the Gufeng area, northern Tibet: Implications for the opening and early evolution of the Bangong-Nujiang Tethyan Ocean. *Journal of Asian Earth Sciences*, *135*, 35–50. https://doi.org/10.1016/j.jseaes.2016.12.015

Fan, J.-J., Li, C., Xie, C. M., & Wang, M. (2014). Petrology, geochemistry, and geochronology of the Zhonggang ocean island, northern Tibet: Implications for the evolution of the Banggongco-Nujiang oceanic arm of the Neo-Tethys. *International Geology Review*, *56*(12), 1504–1520. https://doi.org/10.1080/00206814.2014.947639

Fan, J.-J., Li, C., Xie, C.-M., Wang, M., & Chen, J.-W. (2015). The evolution of the Bangong-Nujiang Neo-Tethys ocean: Evidence from zircon U-Pb and Lu-Hf isotopic analyses of Early Cretaceous oceanic islands and ophiolites. *Tectonophysics*, *655*, 27–40. https://doi.org/10.1016/j.tecto.2015.04.019

Garzanti, E. (2016). From static to dynamic provenance analysis—Sedimentary petrology upgraded. *Sedimentary Geology*, *336*, 3–13. https://doi.org/10.1016/j.sedgeo.2015.07.010

Gehrels, G., Kapp, P., DeCelles, P., Pullen, A., Blakey, R., Weislogel, A., et al. (2011). Detrital zircon geochronology of pre-Tertiary strata in the Tibetan-Himalayan orogen. *Tectonics*, *30*, TC5016. https://doi.org/10.1029/2011TC002868

Girardeau, J., Marcoux, J., Allegre, C. J., Bassoullet, J. P., Tang, Y. K., Xiao, X. C., et al. (1984). Tectonic environment and geodynamic significance of the neo-Cimmerian Donqiao Ophiolite, Bangong-Nujiang suture zone, Tibet. *Nature*, *307*(5946), 27–31. https://doi.org/10.1038/307027a0

Guynn, J., Kapp, P., Pullen, A., Heizler, M., Gehrels, G., & Ding, L. (2006). Tibetan basement rocks near Amdo reveal "missing" Mesozoic tectonism along the Bangong suture, central Tibet. *Geology*, *34*(6), 505–508. https://doi.org/10.1130/G22453.1

Hall, R. (2011). Australia-SE Asia collision: Plate tectonics and crustal flow. *Geological Society, London, Special Publications*, *355*(1), 75–109. https://doi.org/10.1144/SP355.5

Harris, R., Sawyer, R., & Audley-Charles, M. (1998). Collisional melange development: Geologic associations of active melange-forming processes with exhumed melange facies in the western Banda orogen, Indonesia. *Tectonics*, *17*(3), 458–479. https://doi.org/10.1029/97TC03083

Hu, X., Garzanti, E., Wang, J., Huang, W., An, W., & Webb, A. (2016). The timing of India-Asia collision onset—Facts, theories, controversies. *Earth-Science Reviews*, *160*, 264–299. https://doi.org/10.1016/j.earscirev.2016.07.014

Huang, Q. S., Shi, R. D., Liu, D. L., Zhang, X. R., Fan, S. Q., & Ding, L. (2013). Os isotopic evidence for a carbonaceous chondritic mantle source for the Nagqu ophiolite from Tibet and its implications. *Chinese Science Bulletin*, *58*(1), 92–98. https://doi.org/10.1007/s11434-012-5384-8

Huang, Q. T., Li, J. F., Xia, B., Yin, Z. X., Zheng, H., Shi, X. L., & Hu, X. C. (2015). Petrology, geochemistry, chronology and geological significance of Jiang Tso ophiolite in middle segment of Bangonghu-Nujiang suture zone, Tibet. *Journal of China University of Geosciences*, *40*(1), 34–48. https://doi.org/10.3799/dqkx.2015.003

Huang, T. T., Xu, J. F., Chen, J. L., Wu, J. B., & Zeng, Y. C. (2017). Sedimentary record of Jurassic northward subduction of the Bangong-Nujiang Ocean: Insights from detrital zircons. *International Geology Review*, *59*(2), 166–184. https://doi.org/10.1080/00206814.2016.1218801

Ingersoll, R. V. (1983). Petrofacies and provenance of late Mesozoic forearc basin, northern and central California. *AAPG Bulletin*, *67*(7), 1125–1142. https://doi.org/10.1306/03B5B713-16D1-11D7-8645000102C1865D

Ingersoll, R. V., Bullard, T. F., Ford, R. L., Grimm, J. P., Pickle, J. D., & Sares, S. W. (1984). The effect of grain size on detrital modes: A test of the Gazzi-Dickinson point-counting method. *Journal of Sedimentary Research*, *55*(4), 616–618. https://doi.org/10.1306/212F8783-2B24-11D7-8648000102C1865D

Institute of Tibetan Geological Survey. (2002). Geological Report of the 1:250, 000 Regional Geological Survey in Baingoin Area (in Chinese).

Institute of Tibetan Geological Survey. (2006). Geological report of the 1:250,000 Regional Geological Survey in Angdaerco Area (in Chinese).

Isozaki, Y., Aoki, K., Nakama, T., & Yanai, S. (2010). New insight into a subduction-related orogen: A reappraisal of the geotectonic framework and evolution of the Japanese Islands. *Gondwana Research*, *18*(1), 82–105. https://doi.org/10.1016/j.gr.2010.02.015

Jackson, S. E., Pearson, N. J., Griffin, W. L., & Belousova, E. A. (2004). The application of laser ablation-inductively coupled plasma-mass spectrometry to in situ U-Pb zircon geochronology. *Chemical Geology*, *211*(1–2), 47–69. https://doi.org/10.1016/j.chemgeo.2004.06.017

Jacobson, M. I. (1978). Petrologic variation in Franciscan sandstone from the Diablo Range, California. In D. G. Howell, & K. A. McDougall (Eds.), *Mesozoic paleogeography of the western United States, Pacific Coast Paleogeography Symposium 2* (pp. 401–417). Pacific Section, Los Angeles, USA: Society of Economic Paleontologists and Mineralogists.

Kapp, P., & DeCelles, P. G. (2019). Mesozoic-Cenozoic geological evolution of the Himalayan-Tibetan orogen and working tectonic hypotheses. *American Journal of Science*, *319*(3), 159–254. https://doi.org/10.2475/03.2019.01

Kapp, P., DeCelles, P. G., Gehrels, G. E., Heizier, M., & Ding, L. (2007). Geological records of the Lhasa-Qiangtang and Indo-Asian collisions in the Nima area of central Tibet. *Geological Society of America Bulletin*, *119*(7–8), 917–933. https://doi.org/10.1130/b26033.1

Kapp, P., Yin, A., Manning, C. E., Harrison, T. M., Taylor, M. H., & Ding, L. (2003). Tectonic evolution of the early Mesozoic blueschist-bearing Qiangtang metamorphic belt, central Tibet. *Tectonics*, *22*(4), 1043. https://doi.org/10.1029/2002TC001383

Kneller, B. C., & Branney, M. J. (1995). Sustained high-density turbidity currents and the deposition of thick massive sands. *Sedimentology*, *42*(4), 607–616. https://doi.org/10.1111/j.1365-3091.1995.tb00395.x

Lai, W., Hu, X., Garzanti, E., Sun, G., Garzione, C. N., BouDagher Fadel, M., & Ma, A. (2019). Initial growth of the Northern Lhasaplano, Tibetan Plateau in the early Late Cretaceous (ca. 92 Ma). *GSA Bulletin*, *131*(11–12), 1823–1836. https://doi.org/10.1130/B35124.1

Lai, W., Hu, X., Garzanti, E., Xu, Y., Ma, A., & Li, W. (2019). Early Cretaceous sedimentary evolution of the northern Lhasa terrane and the timing of initial Lhasa-Qiangtang collision. *Gondwana Research*, *73*, 136–152. https://doi.org/10.1016/j.gr.2019.03.016

Leier, A. L., DeCelles, P. G., Kapp, P., & Gehrels, G. E. (2007). Lower Cretaceous strata in the Lhasa Terrane, Tibet, with implications for understanding the early tectonic history of the Tibetan Plateau. *Journal of Sedimentary Research*, *77*(10), 809–825. https://doi.org/10.2110/jsr.2007.078

Leier, A. L., Kapp, P., Gehrels, G. E., & DeCelles, P. G. (2007). Detrital zircon geochronology of Carboniferous-Cretaceous strata in the Lhasa terrane, Southern Tibet. *Basin Research*, *19*(3), 361–378. https://doi.org/10.1111/j.1365-2117.2007.00330.x

Li, C. (1987). The Longmucuo-Shuanghu-Lanchangjiang plate suture and the north boundary of distribution of Gondwana facies Permian-Carboniferous system in northern Xizang, China (in Chinese with English abstract). *Journal of Changchun University of Earth Science*, *17*(2), 155–166.

Li, C., Wang, G., Zhao, Z., Du, J., Ma, X., & Zheng, Y. (2019). Late Mesozoic tectonic evolution of the central Bangong-Nujiang Suture Zone, central Tibetan Plateau. *International Geology Review*, 1–24. https://doi.org/10.1080/00206814.2019.1697859

Li, G. W., Sandiford, M., Liu, X. H., Xu, Z. Q., Wei, L. J., & Li, H. Q. (2014). Provenance of Late Triassic sediments in central Lhasa terrane, Tibet and its implication. *Gondwana Research*, *25*(4), 1680–1689. https://doi.org/10.1016/j.gr.2013.06.019

Li, J. F., Xia, B., Xia, L. Z., Xu, L. F., Liu, W. L., Cai, Z. R., & Yang, Z. Q. (2013). Geochronology of the Dong Tso ophiolite and the tectonic environment. *Acta Geologica Sinica (English Edition)*, *87*(6), 1604–1616. https://doi.org/10.1111/1755-6724.12162

Li, N., Hao, H., Gu, Q., Wang, D., & Hu, X. (2017). A transfer learning method for automatic identification of sandstone microscopic images. *Computers & Geosciences*, *103*, 111–121. https://doi.org/10.1016/j.cageo.2017.03.007

Li, S., Ding, L., Guilmette, C., Fu, J. J., Xu, Q., Yue, Y. H., & Pinto, R. H. (2017). The subduction-accretion history of the Bangong-Nujiang Ocean: Constraints from provenance and geochronology of the Mesozoic strata near Gaize, Central Tibet. *Tectonophysics*, *702*, 42–60. https://doi.org/10.1016/j.tecto.2017.02.023

Li, S., Yin, C., Guilmette, C., Ding, L., & Zhang, J. (2019). Birth and demise of the Bangong-Nujiang Tethyan Ocean: A review from the Gerze area of central Tibet. *Earth-Science Reviews*, *198*, 102907. https://doi.org/10.1016/j.earscirev.2019.102907

Li, S. M., Wang, Q., Zhu, D. C., Cawood, P. A., Stern, R. J., Weinberg, R., et al. (2020). Reconciling orogenic drivers for the evolution of the Bangong-Nujiang Tethys during Middle-Late Jurassic. *Tectonics*, *39*, e2019TC005951. https://doi.org/10.1029/2019TC005951

Liang, X., Wang, G., Yuan, G., & Liu, Y. (2012). Structural sequence and geochronology of the Qomo Ri accretionary complex, Central Qiangtang, Tibet: Implications for the Late Triassic subduction of the Paleo-Tethys Ocean. *Gondwana Research*, *22*(2), 470–481. https://doi.org/10.1016/j.gr.2011.11.012

Liu, T., Zhai, Q.-G., Wang, J., Bao, P.-S., Qiangba, Z., Tang, S.-H., & Tang, Y. (2016). Tectonic significance of the Dongqiao ophiolite in the north-central Tibetan plateau: Evidence from zircon dating, petrological, geochemical and Sr-Nd-Hf isotopic characterization. *Journal of Asian Earth Sciences*, *116*, 139–154. https://doi.org/10.1016/j.jseaes.2015.11.014

Ludwig, K. (2008). *Isoplot version 4.15: a geochronological toolkit for Microsoft Excel*. *Berkeley Geochronology Center, Special Publication* (Vol. 4).

Ma, A., Hu, X., Garzanti, E., Han, Z., & Lai, W. (2017). Sedimentary and tectonic evolution of the southern Qiangtang basin: Implications for the Lhasa-Qiangtang collision timing. *Journal of Geophysical Research: Solid Earth*, *122*, 4790–4813. https://doi.org/10.1002/2017JB014211

Ma, A., Hu, X., Kapp, P., BouDagher-Fadel, M., & Lai, W. (2020). Pre-Oxfordian (>163 Ma) ophiolite obduction in central Tibet. *Geophysical Research Letters*, *47*, e2019GL086650. https://doi.org/10.1029/2019GL086650

Ma, A., Hu, X., Kapp, P., Han, Z., Lai, W., & BouDagher-Fadel, M. (2018). The disappearance of a Late Jurassic remnant sea in the southern Qiangtang Block (Shamuluo Formation, Najiangco area): Implications for the tectonic uplift of central Tibet. *Palaeogeography, Palaeoclimatology, Palaeoecology*, *506*, 30–47. https://doi.org/10.1016/j.palaeo.2018.06.005

Marsaglia, K. M., & Ingersoll, R. V. (1992). Compositional trends in arc-related, deep-marine sand and sandstone: A reassessment of magmatic-arc provenance. *Geological Society of America Bulletin*, *104*(12), 1637–1649. https://doi.org/10.1130/0016-7606(1992)104<1637:CTIARD>2.3.CO;2

Metcalf, K., & Kapp, P. (2017). The Yarlung suture mélange, Lopu Range, southern Tibet: Provenance of sandstone blocks and transition from oceanic subduction to continental collision. *Gondwana Research*, *48*, 15–33. https://doi.org/10.1016/j.gr.2017.03.002

Metcalf, K., & Kapp, P. (2019). History of subduction erosion and accretion recorded in the Yarlung Suture Zone, southern Tibet. *Geological Society, London, Special Publications*, *483*(1), 517–554. https://doi.org/10.1144/SP483.12

Murphy, M. A., Yin, A., Harrison, T. M., Dürr, S. B., Chen, Z., Ryerson, F. J., et al. (1997). Did the Indo-Asian collision alone create the Tibetan plateau? *Geology*, *25*(8), 719–722. https://doi.org/10.1130/0091-7613(1998)026<0958:DTIACA>2.3.CO;2

Pullen, A., Kapp, P., Gehrels, G. E., Ding, L., & Zhang, Q. H. (2011). Metamorphic rocks in central Tibet: Lateral variations and implications for crustal structure. *Geological Society of America Bulletin*, *123*(3–4), 585–600. https://doi.org/10.1130/b30154.1

Qu, X., Xin, H., Zhao, Y., & Wang, R. (2010). Opening time of Bangong Lake Middle Tethys oceanic basin of the Tibet Plateau: Constraints from petro-geochemistry and zircon U-Pb LAICPMS dating of mafic ophiolites (in Chinese with English abstract). *Earth Science Frontiers*, *17*(3), 53–63.

Raterman, N. S., Robinson, A. C., & Cowgill, E. S. (2014). Structure and detrital zircon geochronology of the Domar fold-thrust belt: Evidence of pre-Cenozoic crustal thickening of the western Tibetan Plateau. *Geological Society of America Special Papers*, *507*, 89–104. https://doi.org/10.1130/2014.2507(05)

Raymond, L. A. (2019). Perspectives on the roles of mélanges in subduction accretionary complexes: A review. *Gondwana Research*, *74*, 68–89. https://doi.org/10.1016/j.gr.2019.03.005

Searle, M., Windley, B., Coward, M., Cooper, D., Rex, A., Rex, D., et al. (1987). The closing of Tethys and the tectonics of the Himalaya. *Geological Society of America Bulletin*, *98*(6), 678–701. https://doi.org/10.1130/0016-7606(1987)98<678:TCOTAT>2.0.CO;2

Seely, D., Vail, P., & Walton, G. (1974). Trench slope model. In *The geology of continental margins* (pp. 249–260). Verlag, New York: Springer.

Shi, R. (2007). SHRIMP dating of the Bangong Lake SSZ-type ophiolite: Constraints on the closure time of ocean in the Bangong Lake-Nujiang River, northwestern Tibet. *Chinese Science Bulletin*, *52*(7), 936–941. https://doi.org/10.1007/s11434-007-0134-z

Simpson, G. D. (2010). Formation of accretionary prisms influenced by sediment subduction and supplied by sediments from adjacent continents. *Geology*, *38*(2), 131–134. https://doi.org/10.1130/G30461.1

Stern, R. J., & Bloomer, S. H. (1992). Subduction zone infancy: Examples from the Eocene Izu-Bonin-Mariana and Jurassic California arcs. *GSA Bulletin*, *104*(12), 1621–1636. https://doi.org/10.1130/0016-7606(1992)104<1621:SZIEFT>2.3.CO;2

Sun, G., Hu, X., & Sinclair, H. D. (2017). Early Cretaceous palaeogeographic evolution of the Coqen Basin in the Lhasa Terrane, southern Tibetan Plateau. *Palaeogeography, Palaeoclimatology, Palaeoecology*, *485*, 101–118. https://doi.org/10.1016/j.palaeo.2017.06.006

Sun, G., Hu, X., Xu, Y., & BouDagher-Fadel, M. K. (2019). Discovery of Middle Jurassic trench deposits in the Bangong-Nujiang suture zone: Implications for the timing of Lhasa-Qiangtang initial collision. *Tectonophysics*, *750*, 344–358. https://doi.org/10.1016/j.tecto.2018.12.001

Sun, L., Bai, Z., Xun, D., Li, H., & Sun, B. (2011). Geological characteristics and zircon U-Pb SHRIMP dating of the plagiogranite in Amduo ophiolites, Tibet (in Chinese with English abstract). *Geological Survey and Research*, *34*(1), 10–15.

Tang, Y., Zhai, Q., Hu, P., Xiao, X., & Wang, H. (2018). Petrology, geochemistry and geochronology of the Zhongcang ophiolite, northern Tibet: Implications for the evolution of the Bangong-Nujiang Ocean. *Geoscience Frontiers*, *9*(5), 1369–1381. https://doi.org/10.1016/j.gsf.2018.05.007

Tang, Y., Zhai, Q.-G., Hu, P.-Y., Wang, J., Xiao, X.-C., Wang, H.-T., et al. (2018). Rodingite from the Beila ophiolite in the Bangong-Nujiang suture zone, northern Tibet: New insights into the formation ofophiolite-related rodingite. *Lithos*, *316-317*, 33–47. https://doi.org/10.1016/j.lithos.2018.07.006

Tate, G. W., McQuarrie, N., van Hinsbergen, D. J., Bakker, R. R., Harris, R., & Jiang, H. (2015). Australia going down under: Quantifying continental subduction during arc-continent accretion in Timor-Leste. *Geosphere*, *11*(6), 1860–1883. https://doi.org/10.1130/GES01144.1

Velbel, M. A. (1985). Mineralogically mature sandstones in accretionary prisms. *Journal of Sedimentary Research*, *55*(5), 685–690. https://doi.org/10.1306/212F87BA-2B24-11D7-8648000102C1865D

Vermeesch, P., Resentini, A., & Garzanti, E. (2016). An R package for statistical provenance analysis. *Sedimentary Geology*, *336*, 14–25. https://doi.org/10.1016/j.sedgeo.2016.01.009

Wakabayashi, J. (1990). Counterclockwise PTt paths from amphibolites, Franciscan Complex, California: Relics from the early stages of subduction zone metamorphism. *The Journal of Geology*, *98*(5), 657–680. https://doi.org/10.1086/629432

Wakabayashi, J. (2015). Anatomy of a subduction complex: Architecture of the Franciscan Complex, California, at multiple length and time scales. *International Geology Review*, *57*(5–8), 669–746. https://doi.org/10.1080/00206814.2014.998728

Wakabayashi, J. (2017). Sedimentary serpentinite and chaotic units of the lower Great Valley Group forearc basin deposits, California: Updates on distribution and characteristics. *International Geology Review*, *59*(5–6), 599–620. https://doi.org/10.1080/00206814.2016.1219679

Wakabayashi, J., Ghatak, A., & Basu, A. R. (2010). Suprasubduction-zone ophiolite generation, emplacement, and initiation of subduction: A perspective from geochemistry, metamorphism, geochronology, and regional geology. *GSA Bulletin*, *122*(9–10), 1548–1568. https://doi.org/10.1130/B30017.1

Walker, R. G. (1978). Deep-water sandstone facies and ancient submarine fans: Models for exploration for stratigraphic traps. *AAPG Bulletin*, *62*(6), 932–966.

Wang, B.-D., Wang, L.-Q., Chung, S.-L., Chen, J.-L., Yin, F.-G., Liu, H., et al. (2016). Evolution of the Bangong-Nujiang Tethyan ocean: Insights from the geochronology and geochemistry of mafic rocks within ophiolites. *Lithos*, *245*, 18–33. https://doi.org/10.1016/j.lithos.2015.07.016

Wang, H.-Q., Ding, L., Kapp, P., Cai, F.-L., Clinkscales, C., Xu, Q., et al. (2018). Earliest Cretaceous accretion of Neo-Tethys oceanic subduction along the Yarlung Zangbo Suture Zone, Sangsang area, southern Tibet. *Tectonophysics*, *744*, 373–389. https://doi.org/10.1016/j.tecto.2018.07.024

Wang, J. (2000). Geological features of the eastern sector of the Bangong Co-Nujiang River Suture Zone: Tethyan evolution. *Acta Geologica Sinica*, *74*(2), 229–235.

Wang, J., & Fu, X. G. (2018). Sedimentary evolution of the Qiangtang Basin (in Chinese with English abstract). *Geology in China*, *45*(2), 237–259.

Wang, J.-G., Wu, F.-Y., Garzanti, E., Hu, X.-M., Ji, W.-Q., Liu, Z.-C., & Liu, X.-C. (2016). Upper Triassic turbidites of the northern Tethyan Himalaya (Langjiexue Group): The terminal of a sediment-routing system sourced in the Gondwanide Orogen. *Gondwana Research*, *34*, 84–98. https://doi.org/10.1016/j.gr.2016.03.005

Wen, S. X. (1979). New stratigraphic materials in northern Tibet (in Chinese). *Acta Stratigraphica Sinica*, *3*(2), 150–156.

Wu, Y., Cheng, S. Y., Qin, M. K., Guo, D. F., Guo, G. L., Zhang, C., & Yang, J. S. (2018). Zircon U-Pb ages of Dongcuo ophiolite in western Bangonghu-Nujiang suture zone and their geological significance (in Chinese with English abstract). *Earth Science*, *43*(4).

Xia, B., Xu, L., Wei, Z., Zhang, Y., Wang, R., Li, J., & Wang, Y. (2008). SHRIMP zircon dating of gabbro from the Dongqiao ophiolite in Tibet and its geological implications (in Chinese with English abstract). *Acta Geologica Sinica*, *82*(4), 528–531.

Xizang Bureau of Geology and Mineral Resources (XZBGM) (1997). *Lithostratigraphy of Xizang (Tibet) Autonomous Region (in Chinese with English abstract)* (p. 302). Beijing: China University of Geosciences press company.

Xu, M., Li, C., Xu, W., Xie, C., Hu, P., & Wang, M. (2014). Petrology, geochemistry and geochronology of gabbros from the Zhongcang ophiolitic mélange, central Tibet: Implications for an intra-oceanic subduction zone within the Neo-Tethys Ocean. *Journal of Earth Science*, *25*(2), 224–240. https://doi.org/10.1007/s12583-014-0419-5

Yang, J., Xu, Z., Li, Z., Xu, X., Li, T., Ren, Y., et al. (2009). Discovery of an eclogite belt in the Lhasa block, Tibet: A new border for Paleo-Tethys? *Journal of Asian Earth Sciences*, *34*(1), 76–89. https://doi.org/10.1016/j.jseaes.2008.04.001

Yin, A., & Harrison, T. M. (2000). Geologic evolution of the Himalayan-Tibetan orogen. *Annual Review of Earth and Planetary Sciences*, *28*(1), 211–280. https://doi.org/10.1146/annurev.earth.28.1.211

Zeng, M., Zhang, X., Cao, H., Ettensohn, F. R., Cheng, W., & Lang, X. (2016). Late Triassic initial subduction of the Bangong-Nujiang Ocean beneath Qiangtang revealed: Stratigraphic and geochronological evidence from Gaize, Tibet. *Basin Research*, *28*(1), 147–157. https://doi.org/10.1111/bre.12105

Zhai, Q. G., Jahn, B., Wang, J., Hu, P. Y., Chung, S. L., Lee, H. Y., et al. (2016). Oldest Paleo-Tethyan ophiolitic melange in the Tibetan Plateau. *Geological Society of America Bulletin*, *128*(3–4), 355–373. https://doi.org/10.1130/b31296.1

Zhang, K.-J., Cai, J.-X., Zhang, Y.-X., & Zhao, T.-P. (2006). Eclogites from central Qiangtang, northern Tibet (China) and tectonic implications. *Earth and Planetary Science Letters*, *245*(3-4), 722–729. https://doi.org/10.1016/j.epsl.2006.02.025

Zhang, K. J., Xia, B., Zhang, Y. X., Liu, W. L., Zeng, L., Li, J. F., & Xu, L. F. (2014). Central Tibetan Meso-Tethyan oceanic plateau. *Lithos*, *210-211*, 278–288. https://doi.org/10.1016/j.lithos.2014.09.004

Zhang, Y.-C., Shen, S.-Z., Zhang, Y.-J., Zhu, T.-X., An, X.-Y., Huang, B.-X., et al. (2018). Middle Permian foraminifers from the Zhabuye and Xiadong areas in the central Lhasa Block and their paleobiogeographic implications. *Journal of Asian Earth Sciences*, *175*, 109–120. https://doi.org/10.1016/j.jseaes.2018.01.008

Zhang, Y. X., Zhang, K. J., Li, B., Wang, Y., Wei, Q. G., & Tang, X. C. (2007). Zircon SHRIMP U-Pb geochronology and petrogenesis of the plagiogranites from the Lagkor Lake ophiolite, Gerze, Tibet, China. *Chinese Science Bulletin*, *52*(5), 651–659. https://doi.org/10.1007/s11434-007-0084-5

Zhong, Y., Liu, W.-L., Xia, B., Liu, J.-N., Guan, Y., Yin, Z.-X., & Huang, Q.-T. (2017). Geochemistry and geochronology of the Mesozoic Lanong ophiolitic mélange, northern Tibet: Implications for petrogenesis and tectonic evolution. *Lithos*, *292-293*, 111–131. https://doi.org/10.1016/j.lithos.2017.09.003

Zhu, D., Pan, G., Mo, X., Wang, L., Zhao, Z., Liao, Z., et al. (2006). Identification for the Mesozoic OIB-type basalts in central Qinghai-Tibetan Plateau: Geochronology, geochemistry and their tectonic setting (in Chinese with English abstract). *Acta Geologica Sinica*, *80*(9), 1312–1328.

Zhu, D.-C., Li, S.-M., Cawood, P. A., Wang, Q., Zhao, Z.-D., Liu, S.-A., & Wang, L.-Q. (2016). Assembly of the Lhasa and Qiangtang terranes in central Tibet by divergent double subduction. *Lithos*, *34*(1), 59–65. https://doi.org/10.1139/e17-005

Zhu, D.-C., Zhao, Z.-D., Niu, Y., Mo, X.-X., Chung, S.-L., Hou, Z.-Q., et al. (2011). The Lhasa Terrane: Record of a microcontinent and its histories of drift and growth. *Earth and Planetary Science Letters*, *301*(1-2), 241–255. https://doi.org/10.1016/j.epsl.2010.11.005